PERGAMON

Planetary and Space Science 48 (2000) 753–774

Planetary and Space Science

www.elsevier.nl/locate/planspasci

A similarity model for the windy jovian thermocline

Michael Allison

NASA, Goddard Institute for Space Studies, 2880 Broadway, New York, NY 10025, USA

Received 3 November 1998; received in revised form 15 November 1999; accepted 11 January 2000

Abstract

A new conceptual model for the observed banded wind structure of the giant outer planets is proposed, assuming a smoothly distributed potential vorticity (PV) atop a layer of deeply seated, latitudinally variable stratification. With a vanishing horizontal entropy contrast presumably enforced at the bottom of the flow layer by the underlying convection, the thermal-wind balance of observed cloud-top motions implies a mapping of constant potential temperature surfaces, nearly vertical at upper tropospheric levels, down to a deeper, flatter, but variably sloped "thermocline". For a generally colder-poleward distribution of isentropes consistent with the strong equatorial jets of both Jupiter and Saturn, this kind of mapping would also imply a poleward decreasing static stability. The proposed temperature-stability distribution is just the reverse of the Earth's troposphere, where the strongest latitudinal potential temperature gradients are at the bottom instead of the top, with static stability generally increasing toward the pole. The warmer–stabler correlation for Jupiter would be consistent, however, with a nearly monotonic distribution of PV from low to high latitudes, over planetary scales for which the planetary vorticity dominates the relative vorticity of the jets. In this way efficient PV mixing for the isentropically bounded thermocline can account for the dynamical maintenance of the cyclonic flanks of the equatorial jet. Over latitudinal intervals comparable to the internal deformation scale, however, the gradient of the absolute vorticity is dominated by the flow curvature, correlated for a well-mixed PV distribution with the local latitudinal gradient of the static stability, itself proportional for the assumed thermocline structure to the local potential temperature gradient and therefore the local departures in geostrophic velocity. The resulting correlation of velocities and vorticity gradients would imply an alternation of the flow over the internal deformation radius set by the vertical entropy contrast. The requisite size of the deep stability is itself roughly consistent with the diagnostic interpretation of the apparent dispersive character and vertical wavelength of observed temperature oscillations in Jupiter's upper troposphere and stratosphere, as well as a plausible extrapolation of the deep sub-adiabatic lapse rate detected by the Galileo probe. Published by Elsevier Science Ltd.

1. The problem

The observed cloud-tracked wind motions of Jupiter and Saturn continue to pose an outstanding problem for the theory of planetary fluid dynamics. The fundamental puzzle underlying all others is the maintenance of their counterflowing jet streams, as emphasized by Gierasch and Conrath (1993). Both planets appear to be dominated by a quasi-axisymmetric flow structure, but differ in the strength and latitudinal distribution of their zonal mean velocities. Both exhibit super-rotational equatorial jets (exceeding the underlying rotation velocity of their planetary magnetic fields, presumably tied to their deep interiors), with speeds of some 100 and 400 m s^{-1}, respectively, along with alternating jets at higher latitudes.

More than 30 years of theoretical, numerical, and laboratory modeling have been devoted to jovian circulation studies, variously invoking baroclinic instability (e.g. Stone, 1967, 1971; Droegemeier and Sasamori, 1983; Read, 1986a), large-scale latent heat exchange (Barcilon and Gierasch, 1970; Gierasch, 1976), two-dimensional turbulent vorticity transfer (e.g. Williams, 1978; Cho and Polvani, 1996), and convectively driven jets, either in a shallow layer (Condie and Rhines, 1994) or in deep coaxial cylinders (e.g. Ingersoll and Pollard, 1982; Busse, 1983a, b; Sun et al., 1993; Zhang and Schubert, 1996).

0032-0633/00/$ - see front matter Published by Elsevier Science Ltd.
PII: S0032-0633(00)00032-5

At the high end of technical sophistication, the various studies of banded vortical structures spontaneously emerging in numerical integrations of barotropic, shallow water models, as well as the viscous equilibrium of convective rotation achieved via the adjusted balance of parameterized Reynolds stresses in deep cylinder models, have vividly illustrated the organizational character of two-dimensional turbulence. Still unanswered in any fundamental way, however, are the most important questions posed by the puzzle of the Jupiter/Saturn wind systems. What causes the east/west alternation of the observed jet streams over some $(2\pi\times)2000$ and 3000 km on Jupiter and Saturn, respectively? Why do their latitudinal curvatures exceed by a factor of three or more the shear-stability limit for barotropic flow? Why do the equatorial winds of Jupiter (and Saturn) blow from west to east at some 150 (and 500) m/s? Why are the visually brightest cloudy swirling regions mostly anticyclonic rather than cyclonic as on the Earth? It seems fair to suggest that no cogent and comprehensible theory, taking a realistic account of the deep thermal/dynamical structure as related to key parameters, has yet provided either a conceptual or a quantitative answer to these questions.

Some progress has been made in the identification of certain diagnostic scaling relations likely to be of controlling importance for the zonal circulation balance. It has long been recognized that the speed U and horizontal scale L of the jovian winds are characterized by a very small Rossby number ($Ro = U/\Omega L$) measuring the relative strength of the inertial and Coriolis accelerations on a planet with a rotational frequency Ω (e.g. Hide, 1966). The observed zonal wind profiles, as well as numerical experiments with two-dimensional (barotropic/shallow water) models, also imply a horizontal organization for the jovian current systems comparable to the "beta radius" $L_\beta \simeq (U/\beta)^{1/2}$, where U is the zonal velocity and $\beta = 2\Omega\cos\lambda/a$ is the planetary vorticity gradient at latitude λ (with a denoting the planetary radius). A second condition on the zonal velocity and associated length scale could be set by either the horizontal or vertical temperature–density contrast, via the geostrophic thermal wind balance or the baroclinic deformation radius (cf Gierasch and Conrath, 1993). Simple estimates of the possible size of these likely to be imposed by the latent heat release and differentiated molecular weight of a deep water cloud are tantalizingly comparable to the diagnostic requirements, at least in the case of Jupiter, but have so far eluded the incorporation of a predictive model. Of course the atmospheric stratification is well defined for the accessibly measured tropopause and stratosphere regions. While it may be tempting to take as a given external parameter the apparent near-coincidence of the associated deformation scale at these levels with the horizontal jet spacing (or to take the stratospheric scale height as the thickness of a one-layer model), Gierasch and Conrath warn that the vertical structure at these levels is unlikely to provide a responsible control for the cloud-tracked winds below. Similarly, the infrared measurements near the tropopause reveal little more than the apparent reduction in the strength of jets aloft, as inferred by the correlated latitudinal temperature gradient and vorticity at these levels (e.g. Gierasch et al., 1986), and the measured vertical profile of Jupiter's equatorial jet by the Galileo Doppler wind experiment (Atkinson et al., 1998) suggests that this trend toward weaker flow above may begin as deep as 4 bars.

Again, the essential difficulty hinges upon the uncertainty as to the wind, temperature and compositional structure below the visible cloud deck, not directly accessible to the remote sensing observations thus far afforded by planetary spacecraft, and only locally characterized by the Galileo probe down to a level near the end of its telemetry link where the static stability and water abundance are apparently increasing with depth toward as yet unknown values (cf Young, 1998). Nevertheless, Gierasch and Conrath have argued that "the gross dynamical parameters, such as density stratification and rotation rate, are the keys to their behaviors, rather than the particular specifics of radiative forcing, cloud distributions, (or) thermodynamic transformations". If this view is correct, then a simple parametric model for the conceptual understanding of the outer planet circulations must be regarded as a worthwhile prospect.

Are there any overlooked or as yet unaccounted clues to the parametric understanding of the jovian atmospheres? Gierasch (1976) argued that the jovian meteorology may be characterized by a unique regime in which the vertical variation of the potential temperature is small compared with its horizontal variation over latitude, implying nearly vertical isentropes (as mapped with an aspect ratio on the order of the pressure scale height/planetary radius) and a two-dimensional motion field consistent with the apparent beta scaling for the spacing and velocity of the jets. More recently, Allison et al. (1995) showed that the inertial stability of the measured equatorial jet profiles of the giant planets imply a Richardson number (the squared ratio of the Brunt–Vaisäla frequency to the vertical wind shear per scale height) $Ri < 1/Ro_G = 2\Omega a\cos\lambda/U$, consistent with the vertical isentropic configuration characteristic of the conjectured regime, peculiar to the jovian atmospheres.

The diagnostic study of the observed spatial–temporal behavior of waves on Jupiter provides some constraints on the static stability at deeper levels. The very existence of large-scale (Rossby wave) features in Jupiter's equatorial atmosphere apparently drifting to the

west with respect to the zonal mean flow (Maxworthy, 1985; Allison, 1990; Ortiz et al., 1998) implies that these at least are configured in a "shallow" (hydrostatic) layer of a small vertical-to-horizontal aspect ratio, since the propagation of planetary-scale waves within a deep cylindrical geometry would instead be toward the east (Leovy, 1985; Ingersoll and Miller, 1986). Moreover, the diagnostic estimates by Allison (1990) and Ortiz et al. (1998) of the static stability required for the tropospheric ducting of these equatorial waves are roughly consistent with related estimates by Ingersoll and Kanamori (1995) for the expanding propagation of the mid-latitude Shoemaker–Levy (SL9) impacts as apparent ("shallow water") gravity waves. They are also consistent with plausible constraints on the westward drift of Jupiter's Great Red Spot and White Oval features, interpreted as solitary vortices (Williams and Yamagata, 1984; Williams and Wilson, 1988). Taken together, these wave feature diagnostics for several independent observations strongly suggest a hydrostatic and effectively horizontal flow system, with an internal deformation scale comparable to the spacing of the jets. Most recently, the final analysis of data from the Atmospheric Structure Instrument on the Galileo probe at pressures greater than 15 bar (Seiff et al., 1998) "indicate a significant sub-adiabatic temperature gradient by up to 0.5 K/km at 22 bars". The accumulated evidence and now the *in situ* observation of a statically stable region in Jupiter's deep atmosphere, presumably overlying a convective interior, represents both a challenge and an opportunity for the formulation of a comprehensible theory for the jovian circulation.

2. PV-Θ perspective mapping

The thermodynamic state of the atmospheric motion field is conveniently mapped as *potential temperature* $\Theta \equiv T(p_0/p)^{\kappa}$ representing the kinetic temperature of a parcel at a pressure p brought adiabatically and reversibly to a reference level p_0, with $\kappa \equiv R/c_p$ the ratio of the gas constant to the specific heat at constant pressure (Bohren and Albrecht, 1998). Maps of Θ, strictly proportional to the logarithm of the entropy, provide a ready visualization of isentropic layering. Although for terrestrial purposes p_0 is usually defined as the 1000 mb mean surface pressure, in extraterrestrial applications it is important to remember that the potential temperature is really a gauge function specifically calibrated in terms of a particular, but perhaps different reference pressure, which must be factored into a comparison of numerical values or the conversion to kinetic temperatures as these pertain to different models or atmospheres.

As suggested by the figure on the cover of the text by Pedlosky (1987), iso-layered surfaces of an applicable conserved quantity, such as the potential temperature of an atmosphere, may be regarded as a "reservoir" of vorticity, effectively released wherever these surfaces are pulled apart. The explicit formulation of this quantity, known as the potential vorticity (PV), can to good approximation be represented according to standard notation as $q = \rho^{-1}(\zeta + f)\partial\Theta/\partial z$, essentially the product of the relative plus planetary vorticity and the static stability, divided by the atmospheric density. (Appendix A reviews the exact expression for zonal-mean baroclinic motion, along with the approximate PV formulation for gradient-balanced flow, taking account of the special Richardson–Rossby regime of likely relevance to the Jovian atmosphere.)

Fig. 1(a) depicts the latitude–height structure of the potential temperature and PV for the Earth's northern winter hemisphere, as calculated from the data published by Oort and Rasmusson (1971), using Eq. (A1) as given in the Appendix. Tropospheric temperatures are generally colder-poleward, as for the geostrophic balance of the "sub-tropical jet", with a reversed latitudinal gradient above 200 mb. (Note that this section is arranged with latitude increasing toward the right.) The observations show that the strongest horizontal Θ gradients are at the bottom, where isentropic surfaces hit the ground. Θ necessarily increases upward at all levels (above the ~1 km boundary layer), as for a statically stable atmosphere, but the vertical Θ layering from top to bottom is more pronounced toward the Earth's pole, roughly twice as strong there as over the equator, where the top-to-bottom change in Θ is comparable to the equator-to-pole contrast at the surface.

Hoskins (1991) offers an insightful interpretation of the associated PV structure as it relates to the general circulation, referring to the 2 PVU surface as a "quasi-conservative tropopause". Sun and Lindzen (1994) emphasize the obliging appearance of PV smoothing along isentropes within the extratropical troposphere as a basis for the parameterization of the baroclinic eddies. Within the tropics, however, PV surfaces cut sharply across the isentropes. Hoskins notes that it is presumably only "by chance" that the lowest (300 K) isentrope to intersect the dynamical tropopause at 2 PVU also just grazes the Earth's surface in the tropics. But notice that at and below 200 mb, and within the "sub-tropical" region bounded by the westerly jet, the PV is less than half its polar value at the same levels, and only slowly increasing poleward of 40° latitude. Panel (b) of Fig. 1 shows the essentially smooth latitudinal variation of the Ertel PV at the 200 and 350 mb levels. This behavior contrasts with that above the tropopause, where the PV varies rapidly over latitude even near the equator.

As emphasized by Hoskins et al. (1985), the global distribution of the Ertel PV, together with some con-

straint on the mass under the isentropic surfaces and appropriate boundary conditions, permit the deduction of the wind and temperature fields. This so-called "invertibility" principle suggests that the PV framework could enable a geometrical understanding of planetary atmospheric circulations. Although the Earth is so far the only planet for which detailed PV distributions are actually measured, Allison et al. (1994) have presented evidence that the very different atmospheric circulations of Venus and Titan may be approximated by the limit of zero PV within the latitudes of their wind maxima. Barnes and Haberle (1996) have shown the results of numerical modeling experiments suggesting a similar low-PV state across the wide Hadley cell of Mars. As added to recent and related historical thinking about atmospheric vortices and oceanic currents (e.g. Eliassen and Kleinschmidt, 1957; Huang and Stommel, 1990; Polvani et al., 1990), these results encourage a consideration of the possibility that the jovian jet streams are also configured by some well-mixed distribution of PV. A specific modeled account of this and the way it will likely differ from the more familiar terrestrial systems must, however, reflect the likely vertical/latitudinal distribution of potential temperature for a wind layer bounded from below by a convective fluid interior.

3. A jovian thermocline model

Fig. 2 illustrates a possible configuration for the likely very different latitude–height structure of Jupiter's atmosphere, consistent with the modeled vertical structure shown in Fig. 3. If the zonal winds are confined to a "shallow" region (of a small depth compared to the ~2000 km horizontal scale of the motion), then in the absence of a rigid lower boundary within a fully fluid interior, the horizontal entropy gradient must be expected to vanish at the lowest level of the motion, since otherwise the flow would be sheared there. Such a lower, nearly isentropic state could be enforced by the giant planet's internal convection. But the confinement of large-scale motions above some fixed pressure level overlying an isentropic interior also demands a significant horizontal entropy contrast somewhere within the dynamic layer aloft for the geostrophic balance of the zonal currents. For vertically hydrostatic, pressure-balanced flow, and for the small Rossby number regime characteristic of Jupiter's zonal winds, with $U/2\Omega a\cos\lambda \ll 1$, the thermal wind equation (A2) reduces to a direct relation between the latitudinal temperature gradient and the vertical wind shear, with $\partial_\lambda T = e^{-\kappa z^*}\partial_\lambda \Theta \approx -(2\Omega a \sin\lambda/R)\partial_{z^*}U$, using a subscripted λ and z^* to indicate partial differentiation

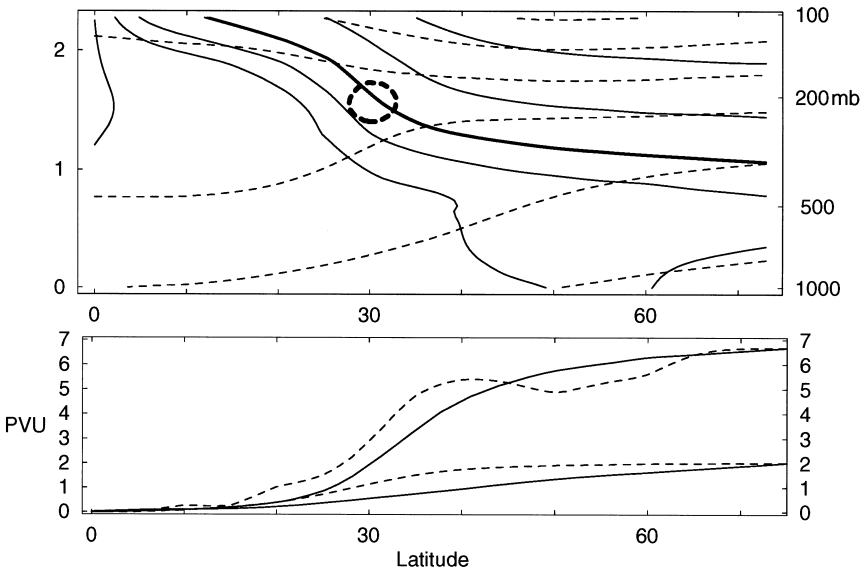

Fig. 1. (a) Latitude–height section of the zonal-mean potential temperature and Ertel PV for the Earth's northern winter hemisphere. Θ is contoured in dashed 30 K increments, increasing upward from 270 K just above the polar surface. Solid contours of PV show surfaces of 0, 0.5, 1, 2, 5, and 10 PVU, increasing poleward (1 PVU $= 10^{-6}$ m^2 s^{-1} K). The 2 PVU surface, shown as a heavy line, may be regarded as a "dynamical tropopause" intersecting the dashed circle marking the 38 m s^{-1} isotach for the westerly jet at 30° latitude. The thermal tropopause at the inflection in the vertical temperature profile (not shown here) resides at the higher 100 mb level. (b) The latitudinal variation of the Ertel PV shown as solid curves at the 200 mb jet level, with a high-latitude attainment of 6.8 PVU, and the 350 mb level, with a high-latitude attainment of 2 PVU. Dashed curves show for comparison the normalized deficit of the squared latitudinal potential temperature contrast at each level with respect to its value at 75°, i.e. $[1-(\Delta_H\Theta(\lambda)/\Delta_H\Theta(0))^2]q_{75^\circ}$, where $\Delta_H\Theta(\lambda) = \Theta(\lambda) - \Theta(75^\circ)$ calculated from temperature–wind data tabulated in Oort and Rasmusson (1971) up to 75° latitude.

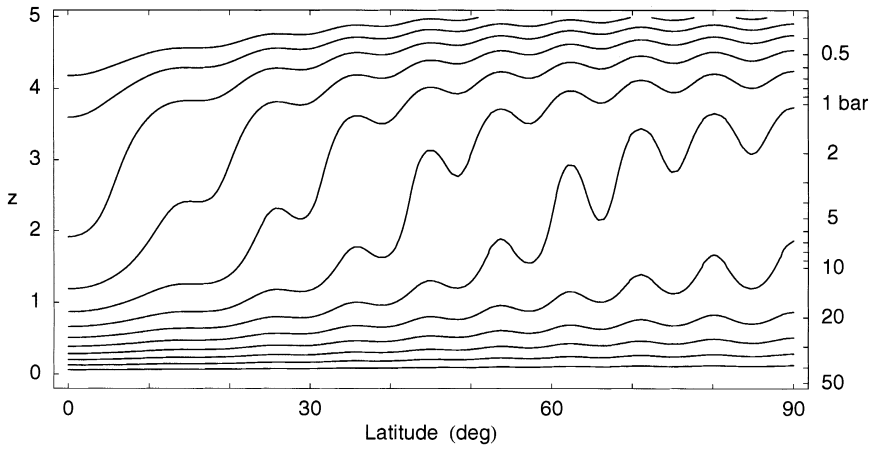

Fig. 2. Schematic illustration for the proposed Jupiter thermocline, showing contours of constant potential temperature in upward-increasing increments of 10 K. The zonal flow layer is presumed to be bounded from below by the interior convection, enforcing a vanishing horizontal temperature contrast at the bottom. Thermal wind balance implies a latitudinal potential temperature contrast aloft and static stability requires a comparable vertical contrast. The resulting correlation between cooler regions and weaker static stability (less compacted vertical layering) is just the reverse of the temperature-stability correlation for the Earth's troposphere shown in Fig. 1.

with respect to latitude and the log-pressure elevation $\ln(p_0/p)$. Horizontal temperature gradients above an isentropic interior also imply vertical stratification above the interface, with static stability requiring a vertical potential temperature contrast at least as large as the equator-to-pole contrast, as illustrated in Fig. 2. But if, as anticipated by Gierasch (1976), the potential temperature within Jupiter's wind layer has a separable vertical/horizontal structure (as it would, for example, in the limit of adiabatic stratification), then the thermal wind shear equation can be vertically integrated and evaluated in terms of $\partial_\chi \Theta$ at some level. Such a special "similarity" structure can be posed in a way that reflects the likely deep seated static stability

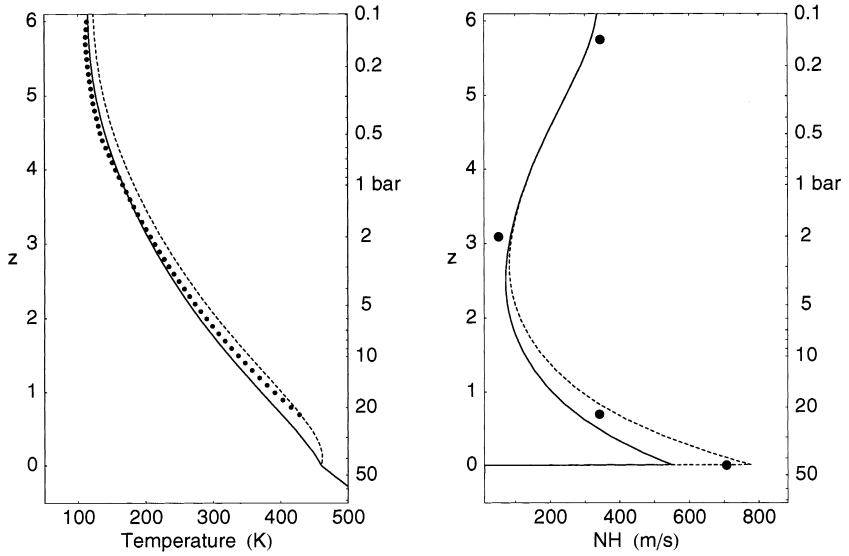

Fig. 3. An example of the modeled vertical profiles of temperature (K) and static stability (NH in m/s) for Jupiter's deep atmosphere, as given by Eqs. (1a) and (1b), assuming a bottom level pressure of 44 bar and $\delta = 0.59$. The dashed curves indicate the (stabler–warmer) equatorial profiles, while the solid curves represent the poles. The extension of the model profiles above 3 bars takes $\theta_{\mathrm{TOP}} = \Delta_T e^{\kappa z^*}\{1 + \tanh[(2/3)(z^* - z_T^*)]\}$ as a simple analytic representation of the upper level variation of the potential temperature, with $\Delta_T \approx \kappa T_{\mathrm{trop}}/(2/3 + \kappa)$, $z_T^* \approx \ln(p_0/0.1\,\mathrm{bar})$, and $T_{\mathrm{trop}} = 124\ \mathrm{K}/2^{1/4}$ (cf Cess and Khetan, 1973). The heavy dotted profile represents the measurements by the Galileo probe Atmospheric Structure Instrument (ASI), as reported by Seiff et al. (1998). The dots in the static stability plot provide a comparison with observational constraints. The topmost dot represents the tropopause at 140 mb, the dot at 2 bar corresponds to the $Ri = 1$ constraint inferred from the vertical shear measured by the Galileo probe (Atkinson et al., 1998), with $NH \geq |\partial U/\partial z^*|$, while the (0.5 K/km) stability at 22 bar is based on the analysis of the deepest data from the Galileo ASI (Seiff et al., 1998). The stability implied by the SL9 waveguide diagnosis by Ingersoll et al. (1995) corresponds to the bottom of a wave guide for the case in which NH increases directly with the pressure, as for the plotted example.

implied by recent observations and constitutes the first essential assumption for the proposed jovian thermocline model, explicitly stated as follows.

Assumption 1. Warmer–stabler similarity structure for the "jovistrophic" flow

Hypothesis: The deep jovian wind layer is configured with an everywhere statically stable, geostrophically balanced, but isentropically lower-bounded thermocline, with a separable vertical/latitudinal linkage of warmer temperatures to stabler stratification of the form

$$\Theta(\lambda, z^*) \equiv e^{\kappa z^*} T(\lambda, z^*)$$
$$= T_0 + [\theta(\lambda) + \Delta\theta](1 - e^{-z^*/\delta}) + \theta_{TOP}(z^*),$$
$$\text{with } \theta(0^\circ) = \Delta\theta \quad \text{and} \quad \theta(\pm 90^\circ) = 0, \tag{1a}$$

so that

$$\Gamma(\lambda, z^*) \equiv R \cdot e^{-\kappa z^*} \partial_{z^*} \Theta$$
$$= (R\Delta\theta/\delta)[1 + \theta(\lambda)/\Delta\theta] e^{-(1/\delta+\kappa)z^*} + \Gamma_{TOP} \tag{1b}$$

and

$$\partial_\lambda \Theta = (1 - e^{-z^*/\delta})\partial_\lambda \theta = -e^{\kappa z^*}(2\Omega a \sin\lambda / R)\partial_{z^*} U \tag{1c}$$

or

$$U(\lambda, z^*) = -(R/2\Omega a \sin\lambda) J(z^*) \partial_\lambda \theta \quad \text{where}$$
$$J(z^*) \equiv \int_0^{z^*} e^{-\kappa z^*}(1 - e^{-z^*/\delta}) dz^*$$
$$= \kappa^{-1}(1 - e^{-\kappa z^*}) - \delta(1 + \kappa\delta)^{-1}[1 - e^{-(1/\delta+\kappa)z^*}]. \tag{1d}$$

T_0 denotes the (assumed constant) temperature at the base of the flow layer at a pressure p_0, $\theta(\lambda)$ the horizontally variable part of the potential temperature field, measuring its departure from the vertical contrast $\Delta\theta$ at the pole, δ the vertical scale for the deep statically stable region, and U the (assumed geostrophic) zonal flow. (The adopted equator-to-pole contrast, $\theta(0) = \Delta\theta$, is chosen for consistency with a second key assumption relating the latitudinal PV distribution to the relative horizontal variation of potential temperature, as specified below.) The static stability for the assumed model is given in terms of $\Gamma \equiv R \cdot e^{-\kappa z^*} \partial\Theta/\partial z^* = R(\partial T/\partial z^* + RT/c_p)$, using the notation defined on p. 61 of the text by Haltiner and Williams (1980), in a form equivalent to the squared product of the Brunt–Vaisäla frequency and the pressure scale height, i.e. with $\Gamma \equiv (NH)^2$, where $N \equiv (g\partial \ln \Theta/\partial z^*)^{1/2}$ and $H \equiv RT/g$. $J(z^*)$ is the vertical "form factor" for the height distribution of the jets. Since this is independent of latitude, the zonal velocity at each level is linked in a self-similar way to that at some evaluated "control level" z_c^* for which the full latitudinal profile can be calculated or observed, with $U(\lambda, z^*) = U_c(\lambda) J(z^*)/J_c$. As evaluated at z_c^*, $J_c \equiv J(z_c^*) \approx \kappa^{-1}(1 - e^{-\kappa z_c^*}) - \delta$, for $\delta \le 1$ and $z_c^* \ge 2$. The last term θ_{TOP} in (1a), and the related Γ_{TOP} in (1b), can be specified as some function of z^* representing the stable stratification near the tropopause, so as to facilitate the plotted extension of the deep modeled structure up to levels near the infrared sounding level, but are assumed to be negligible at pressures greater than ~1–3 bar. Also neglecting vertical variations of the gas constant and specific heat in response to changes in mean molecular weight and the ortho–para hydrogen state, the proposed recipe for the Θ structure will simply fix $\kappa \equiv R/c_p = 0.3$ with $R = 3600\ m^2\ s^{-2}\ K^{-1}$.

Evidence/rationale. Jovian atmospheric wave diagnostics based on the apparent dispersive properties of observed equatorial features (Maxworthy, 1985; Allison, 1990; Ortiz et al., 1998), the westward drift of vortices (e.g. Williams and Yamagata, 1984), and the SL9 shock propagation (Ingersoll and Kanamori, 1995; Hammel et al., 1995) all imply stable stratification at some deep (but hydrostatically "shallow") level, consistent with a deformation scale comparable to the spacing of the counterflowing jets. (A further account is given in Appendix B.) Galileo probe measurements by the Atmospheric Structure Instrument (Seiff et al., 1998) provide further corroboration of a downward-increasing deep static stability below 15 bars, and the measured downward increase of the water mixing ratio suggests a consistent trend in the deep stable layering of mean molecular weight. The assumed static stability at deep levels is likely supported by chemical phase changes (e.g. Barcilon and Gierasch, 1970; Gierasch and Conrath, 1985; Del Genio and McGrattan, 1990) or radiative transport (Guillot et al., 1994). For the particular choice of $\delta = (2-\kappa)^{-1} \approx 0.59$, as for the example shown in Fig. 3, the stability of the deep wind layer (for $z^* < z_T^* - 3$) assumes the simple form of $\Gamma = (R\Delta\theta/\delta)(1 + \theta/\Delta\theta)e^{-2z^*}$, with NH increasing in direct proportion to the pressure, the same as for the tropospheric waveguide of Ingersoll et al. (1994).

The isentropic lower boundary for the assumed horizontal/vertical entropy contrasts aloft would be consistent with convective mixing just below the wind layer, and necessarily implies a direct geometrical linkage between static stability and horizontal temperature contrasts of a form represented in Fig. 2. Although assumed to vanish at the bottom ($z^* = 0$), level, the horizontal Θ gradient as specified by (1c) approaches its full value (somewhere below z_T^*) for $z^* \gg \delta$. The horizontal gradient of *kinetic* temperature for the adopted model, $\partial_\lambda T \equiv e^{-\kappa z^*} \partial_\lambda \Theta$, and therefore also the model vertical wind shear, vanish at $z^* = 0$, but increase to a maximum at a level $z_{max} = \delta \ln[(1/\delta + \kappa)/$

κ]. For $\delta \approx 0.2$–0.6, for example, $z_{max} \approx 0.5-1$, with $(\partial T/\partial\lambda)_{max} \sim 0.7 \times \partial\theta/\partial\lambda$. Above this level, the modeled horizontal temperature gradient and wind shear begin to fall linearly with height. For a flow depth as shallow as 30 bar, the horizontal kinetic temperature gradient at the 150 mb level according to the idealized model would be $(0.15/30)^{0.3}$ or about 1/5 times $\partial\theta/\partial\lambda$ (and still smaller for deeper flows). But if, as the Galileo probe Doppler data suggests, the upper tropospheric decay of the zonal jets modeled by Conrath et al. (1981) should extend below the level where horizontal temperature gradients can be reliably retrieved from infrared measurements, the deep gradients of the jovian thermocline would be entirely hidden from those detectable by available remote sensing.

Assumption 1 provides a similarity relation between the latitude–height potential temperature and the zonal wind field, plausibly consistent with the peculiar features of the jovian flow regime. The assumption of a second temperature–wind relation in terms of the associated PV distribution provides an example of the dynamical closure needed to account for the observed configuration of the zonal jets.

Assumption 2. PV-θ balance for cool-cyclonic shear

Hypothesis: Assume that at some specified level z_c^* the normalized PV of the jovian thermocline, as prescribed by Eq. (A8) in the Appendix, is distributed over latitude as $\Pi_c \equiv \Pi(\lambda, z_c^*) = 1 - (\theta/\Delta\theta)^2$, so that the normalized absolute vorticity matches the deficit of the relative variation of the horizontal potential temperature contrast, i.e.

$$\frac{\Pi_c(\lambda)}{1+\theta/\Delta\theta} = \frac{(f - \partial U_c/a\partial\lambda)}{2\Omega(1+\varepsilon)} = (1-\theta/\Delta\theta)\mathrm{Sign}(\lambda) \qquad (2)$$

with Sign(λ) equal to $+1$, 0, or -1 for λ positive, zero, or negative, where U_c denotes the geostrophic thermal wind at level z_c^* and ε the ratio of the relative to planetary vorticity at the pole.

Evidence/Rationale. At one level this parameterization for the latitudinal variation of the normalized PV Π_c may be regarded as a plausible interpolation providing a functional link to the θ-field for a presumed smooth variation between its given unitary value at the pole, where $\theta/\Delta\theta$ is by definition zero, and the zero equatorial value for symmetric stability (cf Stevens, 1983), as for $\theta/\Delta\theta = 1$. Essentially, the same temperature–vorticity relation would obtain with $\Pi_c = 1$ over a restricted range of mid-to-high latitudes for which $\theta \ll \Delta\theta$. At the level of physical reasoning, (2) may be viewed as a simple recipe for the jovian vorticity–temperature correlations inferred from the diagnostic–geostrophic analysis of the observed wind field. Over the global scale of variation, neglecting the relative vorticity as compared with the planetary vorticity, (2) implies that in low latitudes where $f/2\Omega$ is small, the temperature must be warmer (and the stability larger) as compared with high latitudes where $f/2\Omega$ approaches unity, consistent with the latitudinal geopotential drop for a westerly equatorial jet. In the vicinity of a fixed latitude for which the variation of f can be neglected, the inspection of (2) suggests that cooler regions in the deep wind layer will possess more cyclonic relative vorticity (larger $-\partial U/a\partial\lambda$) than warmer regions, as anticipated by Ingersoll and Cuzzi (1969). The implied stability–vorticity relation is also consistent with that for long-lived anticyclonic vortices numerically simulated by Williams (1997) for a baroclinic jovian atmosphere. (As shown in Fig. 3 of his study, stable anticyclones are both warmer and more stable at depth than their surroundings.) Note that as given (2) is *not* the same as either uniform or "piecewise constant" PV over latitude or along isentropic surfaces. As interpreted for the Earth, with θ and $\Delta\theta$ respectively evaluated as the continuous latitudinal and equator-to-pole contrast in potential temperature at the 200–300 mb level, $1-(\theta/\Delta\theta)^2$ shows a reasonable correlation with the normalized variation of the Ertel PV assessed from actual measurements at the same levels, as shown in Fig. 1(b).

As reviewed above, there are several indications from previous work that the wind field will also be related to the horizontal "beta scale" $(U/\beta_0)^{1/2}$, where $\beta_0 \equiv 2\Omega/a$ characterizes the planetary vorticity gradient. In anticipation of an explicit realization of these linkages in the theory outlined here, the vertically integrated "jovistrophic" thermal wind equation (1d), evaluated at a level z_c^*, can be calibrated in terms of a (constant) "deformation scale" L_D, as

$$\partial_\lambda(\theta/\Delta\theta) = -(\beta_0 L_D^2)^{-1}\sin\lambda \cdot U_c \qquad (3a)$$

where

$$L_D^2 \equiv \beta_0^{-1}\int_0^{\pi/2} U_c(\lambda)\sin\lambda \, d\lambda = (J_c R\Delta\theta)/4\Omega^2. \qquad (3b)$$

Given some choice for the evaluated level z_c^*, and therefore the associated value of J_c, this uniquely specifies the relationship between $\Delta\theta$, L_D and the wind field $U_c(\lambda)$. (For z_c^* anywhere between 2 and 4 scale-heights above the bottom of the flow layer and $\delta \leq 0.6$, for example, J_c would lie in a range of approximately 1–2.) Unlike the familiar usage of quasi-geostrophic theory, with an internal deformation radius defined as NH/f, here L_D is calibrated with respect to the pole, where $f(90^\circ) = 2\Omega$ and the static stability at the bottom of the wind layer is $\Gamma_0 = (R\Delta\theta/\delta)$, so that

by (3) the deformation scale as defined for the jovian thermocline is also given as $L_D=(J_c\delta\Gamma_0)^{1/2}/2\Omega$. But as defined here L_D is uniquely given in terms of the latitudinal integral of $U_c(\lambda)$.

Table 1 summarizes the key parameters for selected jovian thermocline models, including a more shallow (moist–convective?) alternative to the example illustrated in Fig. 3, with fixed choices for their deformation scales, as evaluated with (3b) for their modeled latitudinal profiles presented below. Although the actual depth of the wind layer is not known, p_0 and T_0 must be consistently chosen so that the implied "adiabat", as adjusted by $\Delta\theta$ over a thickness δ, matches on to the observed temperatures aloft, while $\Delta\theta$ in turn depends upon the vertical integration factor J_c for the level z_c^*. At the present time the (perhaps variable) $\sim$0.5–1 bar level for the cloud tracked winds is the only level for which the link between the vertical structure parameters and the latitudinally integrated flow profile can be observationally calibrated. Both the Galileo probe Doppler data and the Voyager infrared measurements suggest that the winds are actually stronger at somewhat deeper levels, therefore likely to be more relevant to the evaluated top of the still deeper region of the stronger-upward shear. (The implied temperature contrasts for the geostrophic balance of stronger flow at deeper levels are necessarily reduced aloft by some dissipative process in concert with the observed shear toward upward-weaker winds.) While many different choices are possible, in order to fix the evaluation and comparison of other parameters for the examples considered here, z_c^* is assumed to coincide with the 3 bar level for the given examples. The results are not greatly different from those for z_c^* fixed at either 2 or 4 bars, owing to the slow variation of the integration factor $J(z^*)$ at upper levels.

A stable layer with a bottom pressure of 44 bar and $\delta \approx 0.6$ (the example shown in Figs. 2 and 3) might be supported by the radiative transfer model of Guillot et al. (1994). Their re-evaluation of Jupiter's deep vertical structure with the most recent opacity data suggests that in the absence of condensed water a statically stable layer could exist between the 200 and 500 K levels. Depending on as yet uncertain opacity contributions of minor metallic constituents, other still deeper stable layers could be supported by efficient radiative transport at levels exceeding tens of kilobars. As noted by Gierasch and Conrath (1985) the condensation of SiH_4 and MgH clouds might also impose statically stable layers at comparably deep levels. Alternatively, a latitudinally variable water cloud for a super-solar oxygen abundance could mediate the required entropy contrasts at the $\sim$25–30 bar level, by some differentiation of both latent heat and mean molecular weight (cf Gierasch and Conrath, 1985; Del Genio and McGrattan, 1990), with the sub-saturated measurement of water by the Galileo mass spectrometer (Niemann et al., 1998) representing a local departure from a larger abundance elsewhere. Banfield et al. (1998) assert a probable identification of an isolated water cloud below 4 bar in Galileo imaging of the Great Red Spot region (necessarily implying a super-solar abundance at that location) while Sromovsky et al. (1998) infer a relative humidity from the probe net flux radiometer less than 10% at all sampled levels. The apparent factor 10 increase of the measured water abundance with increasing depth between 12 and 19 bar at the probe entry site, as reported by Niemann et al. (1998), cannot, however, be explained by the chemical equilibrium of a sub-solar mixture. (A sub-solar water abundance in chemical equilibrium would imply condensation above the 5 bar level with uniformly distributed vapor below inconsistent with a factor 10 increase over scale-height deeper levels.) Although the deep Saturn adiabat (not plotted) is even less constrained by available observations, the extrapolation of its cloud-top temperature implies a colder interior, so that water condensation could occur at

Table 1
Selected examples of vertical structure models for Jupiter and Saturn

Parameter	Jupiter (dry/radiative?)	Jupiter (moist/convective?)	Saturn (moist/convective?)
Deformation scale L_D (km)	1400	1400	2870
Control level pressure p_c (bar)	3	3	3
Bottom pressure p_0 (bar)	44	30	100
Bottom temperature T_0 (K)	460	390	300
Vertical stability scale δ	0.59	0.2	0.59
J_c factor at $z_c^* = \ln(p_0/p_c)$	1.35	1.47	1.7
Deep potential temperature contrast (ref. to p_0) $\Delta\theta$ (K)	50	46	147
Maximum horizontal kinetic temperature contrast (K)	36	39	105
Pressure level of maximum horizontal kinetic temperature contrast (bar)	14	17	33
Horizontal temperature contrast at 150 mb (K)	9	9	21

much deeper levels than on Jupiter with a larger jump in potential temperature consistent with Saturn's stronger winds.

It may be noted that (2) and (3) imply that the latitudinal gradient of the parameterized PV at level z_c^* is $\partial_\lambda \Pi_c \approx 2\sin\lambda(\theta/\Delta\theta)U_c/\beta_0 L_D^2$. Necessarily zero at both the equator and pole, this latitudinal PV gradient would be expected to vary elsewhere in step with wind and temperature variations, but more slowly at high latitudes where $(\theta/\Delta\theta)$ and U_c are relatively small. The latitudinal PV gradient for the adopted parameterization is reminiscent of certain quasi-geostrophic constraints on the "steering level" for baroclinic eddy transports (cf Held, 1982), and might eventually find less speculative placement in this context. It is not necessary that the actual PV gradient assume precisely this form, however, which may need to be modified for Uranus and Neptune. The given PV-Θ recipe merely provides a tractable closure for a simple model of the latitudinal wind profiles of Jupiter and Saturn, illustrating their inertial control in terms of a direct link between their internal deformation scales and the strength and widths of their currents.

4. Latitudinal profiles and sections

Eqs. (2) and (3), as based on assumptions 1 and 2 above, imply a closed system for the latitudinal variation of the potential temperature and the zonal velocity. A simple exposition of the model parameter dependence as applied to Jupiter and Saturn is afforded by its approximate analytic solution. Consider first a *planetary scale regime* for which the relative vorticity is neglected compared with f, as appropriate to the global circulation averaged over the smaller-scale variation of the jets. Then with the assumed neglect of $\partial_\lambda U$ and ε in (2) the PV balance reduces to $\theta/\Delta\theta \approx 1-\sin\lambda$ in the planetary approximation, which with (3) implies that $U_c \approx \beta_0 L_D^2 \cot\lambda$. The implied cyclonic intensification of the westerly flow toward lower latitudes must break down somewhere close to the equator, however, where as $\theta/\Delta\theta$ approaches unity, (2) would instead reduce to $-a^{-1}\partial_\lambda U \approx -f$, as for an anticyclonic shear zone. This may be reasonably supposed to occur where the planetary vorticity f is matched by the assumed negligible relative vorticity of the global cyclonic shear, with $-a^{-1}\partial_\lambda U \approx \beta_0 L_D^2/a\lambda^2 \approx 2\Omega\lambda$ (in the small-angle approximation), at a critical latitude $\lambda_c \approx (L_D/a)^{2/3}$, and a corresponding equatorial velocity $U_e \approx \beta_0 L_D^2/\lambda_c \approx 2\Omega a(L_D/a)^{4/3}$. With $\Omega a = 12{,}568$ m s^{-1} for Jupiter, and a choice of $L_D \approx 1400$ km, comparable to the observed inverse horizontal wavenumber of the high-latitude jets, $U_e \approx 130$ m s^{-1} and $\lambda_c \approx 4^\circ$ latitude. Using $L_D \approx 3000$ km for the somewhat wider spacing of the high-latitude jets on Saturn, where $\Omega a = 9872$ m s^{-1}, the same relations give $U_e \approx 360$ m s^{-1} and $\lambda_c \approx 8^\circ$. Despite some variation among the cloud-tracked wind studies for the equatorial regions of Jupiter and Saturn (e.g. Limaye, 1986; Beebe et al., 1996; Sanchez-Lavega et al., 1993), perhaps owing both to temporal variability and wave dispersions there, these appear to be respectable estimates for the equatorial jets.

An account of the high-latitude alternation of the jets must include the modulation of this rudimentary trend for the global scale motion by their relative vorticity contribution to the total PV balance. Upon the elimination of $\theta/\Delta\theta$ between (2) and (3), the latitudinal variation of the zonal velocity may be specified as

$$d^2U_c/d\lambda^2 + (1+\varepsilon)(a/L_D)^2 \mid \sin\lambda \mid U_c \approx 2\Omega a\cos\lambda \qquad (4)$$

Note that Eq. (4) is neither a restatement of the Charney and Stern (1962) criterion for baroclinic instability, as derived from the terrestrial quasi-geostrophic theory for a horizontally uniform static stability, nor a repetition of the marginal barotropic stability criterion for the shallow water model (cf Williams and Yamagata, 1984), where L_D is given in terms of a constant mean thickness parameter. In contradistinction with the usual criterion for a vanishing quasi-geostrophic PV gradient, with $u_{yy} \approx \beta + U/L_D^2$, here $u_{yy} \approx \beta - U \mid \sin\lambda \mid /L_D^2$, i.e. with the term directly proportional to the flow velocity of the opposite sign as for the usual equivalent barotropic systems. The positive augmentation of the planetary vorticity gradient for easterly (westward) jets admits a much larger latitudinal flow curvature than the barotropic criterion, consistent with cloud-tracked wind observations (Limaye et al., 1986; Ingersoll and Pollard, 1982). This is again a direct consequence of the strongly variable warmer-where-stabler stratification for the assumed jovian thermocline, as opposed to the observed weakly variable cooler–stabler correlation for the terrestrial atmosphere (or the thicker-cyclonic shear correlation for neutral barotropic stability in the shallow water model).

In the vicinity of some fixed mid-latitude λ_0 for which the local variation of $\sin\lambda$ can be neglected, Eq. (4) assumes the form of a simple harmonic oscillator equation for U, implying an alternation of the flow over a horizontal wavelength of $2\pi \cdot L_D/\sqrt{\sin\lambda_0}$. Taking account of the continuous variation, an approximate representation of the implied alternation of velocity over mid- to high-latitudes can be constructed from the sum $U_c/\beta_0 L_D^2 \approx A(\sin\lambda)^{-1/2}\sin[(\sin\lambda)^{1/2}2a\lambda/3L_D] + \cot\lambda$, where A is some constant. This mimics the slow variation of the latitudinal wavenumber of the jets with the approximation $(2a/3L_D)(1+\lambda/2\tan\lambda)(\sin\lambda)^{1/2} \approx (a/L_D)(\sin\lambda)^{1/2}$, so that $d^2U_c/d\lambda^2 \approx -2\Omega a \cdot A(\sin\lambda)^{1/2}\sin[2a\lambda(\sin\lambda)^{1/2}/$

$3L_D]$ + terms of order L_D/a for $\lambda \gg \lambda_c$. Such an approximation clearly demands a parameter setting with $L_D/a \ll 1$, but this appears to be appropriate for both Jupiter and Saturn. Although $(2/3)(1+\lambda/2 \tan \lambda)$ is as small as 2/3 at the pole, it approaches its unitary estimate toward low latitudes where the jet amplitude A (relative to $\beta_0 L_D^2$) can be set by a match to an appropriate equatorial solution. For $\lambda < \lambda_c$, (4) can be approximated as $d^2U_c/d\lambda^2 \approx 2\Omega a - (a/L_D)^2 \lambda \cdot U_e$, where $U_e \equiv U_c(0)$, which for $dU_c/d\lambda = 0$ on the equator integrates to $U_c \approx U_e[1 - (a/L_D)^2 \lambda^3/6] + \Omega a \lambda^2$. This equatorial profile can be matched on to the other at $\lambda = \lambda_c$ (to within the small angle approximation) for $A = (L_D/a)^{-1/3}/2$ and again $U_e \approx 2\Omega a (L_D/a)^{4/3}$. L_D is the only free parameter for this construction, but may itself be regarded as a discrete eigenvalue of the equator-to-pole boundary problem, corresponding to the inverse meridional wavenumber. Since the zonal velocity must by definition vanish at the pole, the deformation scale may be selected as $L_D = a/(6n + 3)$, where n is an integer equal to the number of alternating jet stream pairs away from the equator. For this choice the flow is cyclonically sheared at the pole, with $\varepsilon \approx (L_D/a)^{2/3}/3$. $L_D = a/6n$ would also give a vanishing velocity at the pole, but with an anticyclonic shear there implying an easterly velocity a short distance away and therefore a decrease of $\theta/\Delta\theta$ toward lower latitudes with respect to its defined value of zero, which would be less statically stable. In the real atmosphere the discrete selection of L_D may be mediated by some diffusive readjustment of the actual latitudinal boundaries for the PV mixing.

Then also including in an obvious way small corrections for the estimated value of ε as it appears in (4), the composite analytic expression for the zonal velocity reads

$$U_c \approx \begin{cases} 2\Omega a \left(\dfrac{L_D}{a}\right)^{4/3} \left[1 + \dfrac{1}{2}\left(\dfrac{\lambda}{\lambda_c}\right)^2 - (1+\varepsilon)\dfrac{1}{6}\left(\dfrac{\lambda}{\lambda_c}\right)^3\right] \\ \quad \text{for } \lambda < \lambda_c \equiv (L_D/a)^{2/3} \\ 2\Omega a \left[\dfrac{(1+\varepsilon)\left(\dfrac{L_D}{a}\right)^{5/3}}{2\sqrt{\sin\lambda}} \sin\left[\dfrac{2}{3}\dfrac{a}{L_D}\lambda\sqrt{\sin\lambda}\right] \right. \\ \quad \left. + \left(\dfrac{L_D}{a}\right)^2 \dfrac{\cot\ \lambda}{(1+\varepsilon)}\right] \\ \quad \text{for } \lambda > \lambda_c \end{cases}$$

$$\text{with } L_D = a/(6n+3) \quad \text{and} \quad \varepsilon \approx \lambda_c/3. \tag{5}$$

Table 2
Numerical parameters for the modeled Jupiter and Saturn wind profiles

Parameter	Jupiter	Saturn
External/assumed		
Planetary radius a (km)	71,490	60,270
Planetary (equatorial) rotation speed Ωa (m s^{-1})	12,568	9872
Jet number index n	8	3
Analytic derivations		
Deformation scale		
$L_D = a/(6n + 3)$ (km)	1402	2870
Critical equatorial latitude		
$\lambda_c = (L_D/a)^{2/3}$ (rad)	0.073	0.131
(°)	4.2	7.5
Equatorial wind velocity		
$U_e = 2\Omega a (L_D/a)^{4/3}$ (m s^{-1})	134	339
Equatorial peak velocity		
$U_p = 4U_e/3$ (m s^{-1})	179	452
First easterly/westerly jet latitudes		
$\lambda_{FE} = 3.7\lambda_c$ (°)	15	28
$\lambda_{FW} = 5.2\lambda_c$ (°)	22	39
Zonal jet curvature/$\beta(60°)$		
$U_{yy}/\beta(60°) = (L_D/a)^{-1/3}$	3.7	2.8
Inverse peak global		
Rossby number $Ro_G^{-1} = \Omega a/U_p$	70	22
Estimated polar $\varepsilon \approx (L_D/a)^{2/3}/3$	0.024	0.044
Numerical solution results		
Exact (numerical) ε for $\lvert 1 - \theta(0)/\Delta\theta \rvert < 10^{-5}$	0.15748	0.24250
Equatorial wind velocity (m s^{-1})	149.9	364.2

Given the appropriate planetary size and rotation parameters, as given in Table 2, $n = 8$ and $n = 3$ appear to provide a best match of (5) to Jupiter and Saturn, respectively, as for the latitudinal wind and potential temperature profiles plotted in Figs. 4 and 5. The qualitative resemblance of the modeled profiles to cloud tracked wind data for both planets is apparent (cf Limaye, 1986; Ingersoll et al., 1984). Although (5) cannot be regarded as a mathematically rigorous solution to (4), its approximate fidelity to the model can be tested by its recursive evaluation with the assumed balances from which it is derived. In particular, the fractional difference of the deformation scale given by the square root of the latitudinal integral of the represented profile (5) as defined by (3b) from the incorporated value $L_D = a/(6n + 3)$ is only 0.017 for Jupiter and 0.032 for Saturn. A further test is afforded by the numerical evaluation of $\theta/\Delta\theta$ from the calculated shear for the analytic wind profile in the PV balance Eq. (2), shown as the dashed curves in the potential temperature plots of Figs. 4 and 5. While snugly fitted to the equator, and tolerably matched for the first alternation of the low-latitude jets, this comparison shows its largest discrepancies at λ_c, where the analytic profiles are joined, and near the pole, where the presumed estimation of the latitudinally variable wavenumber is at its worst. The recursively evaluated gradient of θ from the vorticity appears to be roughly half the needed size for a perfect match to the polar jets, and suggests that a more accurate representation of the assumed jovistrophic/PV balance might be attained by a latitudinal profile with a comparably stronger amplitude for the alternating flow. Although (5) can only be regarded as a heuristic representation of the wind profile implied by (4), it provides an analytic realization of both the "planetary-scale" limit of cyclonic shear on the poleward flanks of the equatorial jet and the high-latitude alternation of jets over a horizontal scale comparable to L_D.

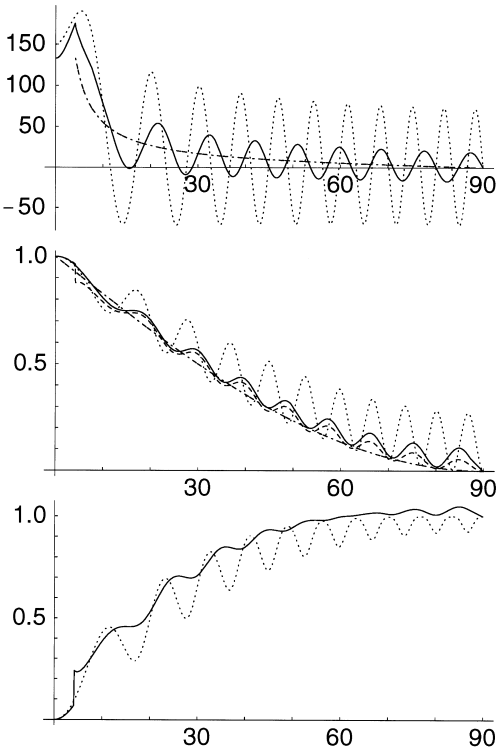

Fig. 4. Modeled latitudinal profiles of the zonal wind, potential temperature, and PV variation for Jupiter with $L_D = 1402$ km. The top portion (a) shows the zonal velocity in m s^{-1} over latitude (in degrees). The solid curve shows the analytic profile (5) for a jet number index $n = 8$, the dash–dot curve the "planetary approximation" to the model with $U_c \approx \beta_0 L_D^2 \cot\lambda$, and the short dashed curve a numerical solution, as described in the text. The middle portion (b) shows the relative potential temperature contrast ($\theta/\Delta\theta$), the solid curve for a numerical integration of Eq. (2) using the analytic profile (5) for the zonal wind, the dash–dot curve the planetary approximation, with $\theta/\Delta\theta \approx 1-\sin\lambda$, and the dashed curve the numerical calculation of $\theta/\Delta\theta$ as the absolute vorticity deficit given by (2) using the analytic expression for the calculation of $a^{-1}\partial_\lambda U_c$. The large-amplitude undulations shown by the short-dashed curve correspond to the numerical solution. The lower portion (c) shows the normalized PV variation, with the solid curve for the analytic profile, and the short dashed curve for the numerical solution.

Figs. 4 and 5 also show for comparison, as the short dotted curves, numerical solutions for the latitudinal wind profiles and potential temperature obtained for the same values of $L_D = a/(6n + 3)$ for each planet, as given in Table 2. These were derived by an iterated in-

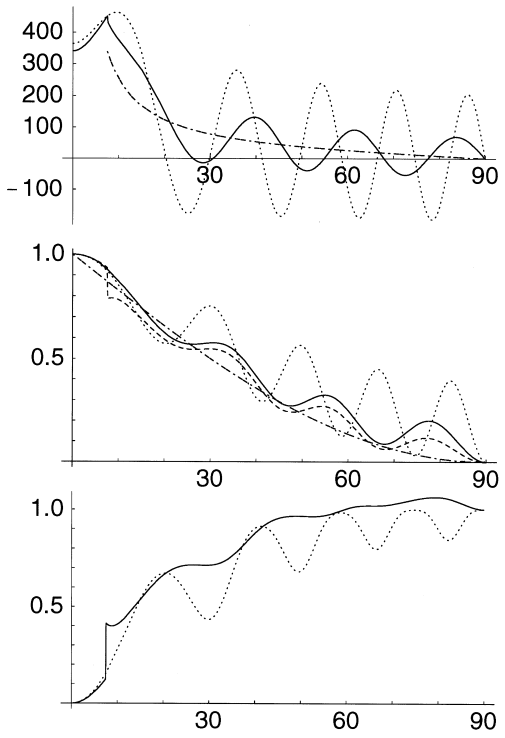

Fig. 5. Modeled latitude profiles of the zonal wind, potential temperature, and PV variation, as in Fig. 4, but for Saturn (note the change in the velocity scale) with $n = 3$ and $L_D = 2870$ km.

tegration of the coupled equations (2) and (3) for the assumed jovistrophic and PV balance, imposing as boundary conditions a vanishing U and θ at the pole. Starting with an initial guess for ε, the result of the coupled integration of $\theta/\Delta\theta$ to the equator was compared against its assumed unitary value there. The iterative correction of ε and the latitudinal integration were repeated until solutions were obtained with $(1-\theta/\Delta\theta) < 10^{-5}$. As shown by the plots, both the total number and the strength of the high-latitude jets obtained by the numerical solutions are larger than for the analytic representations. The search for solutions by the adopted numerical procedure corroborates a discrete selection of admissible deformation parameters, analogous to that inferred for the heuristic solution, with ranges of L_D for which $\theta/\Delta\theta$ cannot be brought to unity. Although not shown here, numerical solutions can, however, be constructed with the same assumed number of high-latitude pairs (eight and three for Jupiter and Saturn), but with deformation scales about 25% larger for each planet, reflecting the underestimate noted above for the polar wavenumber in the analytic approach, and with still stronger jets at high latitudes.

The lower panel (c) in each of Figs. 4 and 5 shows the PV distribution corresponding to both the analytic profile and the numerical solution. Although the baroclinic stability dependence for the generalized Ertel PV or its application here to the assumed jovian thermocline structure has not been established, it might be conjectured that a negative poleward latitudinal gradient is unstable, as in quasi-geostrophic theory. If so, the stable readjustment of the "exact" solution for the idealized PV parameterization might account for the observed mostly weaker jets at high latitudes more in agreement with the analytic representation of Eq. (5).

Despite the apparent discrepancies, the numerical solutions corroborate the qualitative sense of the alternating jets expressed by the heuristic solution and to good quantitative agreement the analytic estimate of the strength and width of the westerly flow at the equator, as well as the differences between Jupiter and Saturn, as primarily related to L_D. [Discrete classes of easterly equatorial jets can also be calculated by the numerical procedure satisfying the assumed boundary conditions and a unitary $\theta/\Delta\theta$ on the equator, but these necessarily correspond to $\theta/\Delta\theta > 1$ at higher latitudes, which by (2) would imply an absolutely inertially unstable profile, with a negative (or positive) PV in the northern (or southern) hemisphere, as established for the general case by Stevens, 1983.] Various features of the flow profile as exposed to good approximation by the heuristic solution and its explicit dependence on L_D or the jet number index are indicated in Table 2. The latitudes of the first easterly and westerly jets away from the equator, for example, occur where the argument of $\sin[(\sin\lambda)^{1/2}2a\lambda/3L_D]$ attains the value of $3\pi/2$ and $5\pi/2$, respectively, i.e. for $\lambda_{FE} \approx (9\pi/4)^{2/3}\lambda_c$ and $\lambda_{FW} \approx (15\pi/4)^{2/3}\lambda_c$ in the small-angle approximation. The ratio of the peak latitudinal flow curvature to the beta parameter is $U_{yy}/\beta \approx (L_D/a)^{-1/3}/2\cos\lambda$ for the analytic profile, attaining values as large as 3.7 and 2.8 at 60° latitude for Jupiter and Saturn, respectively, in rough agreement with that observed for the westerly jets on both planets (Sromovsky et al., 1983; Ingersoll et al., 1984; Limaye et al., 1986) clearly exceeding the barotropic stability limit of $U_{yy} = \beta$. The derived relationship between $\lambda_c = (L_D/a)^{2/3}$, regarded as a characteristic latitudinal scale for the equatorial jets, and their speed, $U_e = 2\Omega a(L_D/a)^{4/3}$, is consistent with the suggestion by Hide (1966) that their width in radians should be of order $(U_e/2\Omega a)^{1/2}$.

Once evaluated, the latitudinal profiles can be used with the thermocline template, as specified by Eqs. (1a)–(1d), to construct meridional–vertical sections of wind, temperature and other quantities of interest, as shown in Figs. 6 and 7. Since with the exception of the fast 163 m s^{-1} jet at 24° north (planetographic) latitude on Jupiter (Limaye, 1986), the observed cloud-tracked winds more nearly resemble the analytic profile, (5) has been adopted for these in an attempt to represent the likely size of the jet-scale contrasts which might be observed there. Again L_D and, therefore, the equator-to-pole $\Delta\theta$ are by construction essentially the same as for the numerical solution, and aside from the artificial kink at the λ_c matching point, the equatorial jets represented by (5) are in good quantitative correspondence with the exact (numerical) solution.

The strong vertical shear indicated for the equatorial region in the modeled Jupiter example clearly exceeds that measured at deep levels by the Galileo Doppler wind experiment (Atkinson et al., 1998). It is not clear, however, to what extent the sampled "hot spot" location at 6.5° planetocentric latitude, apparently typical of only 15% of the surface area of the equatorial region (Young, 1998) can be regarded as an accurate characterization of the vertical shear of the zonal mean flow. While the Galileo Doppler results provide compelling evidence for an equatorial flow depth exceeding 20 bars, as well as an indication (robust to the $1-\sigma$ data level) of some decrease in wind speed with increasing depth between 5 and 12 bars, the actual vertical shear at the entry site almost certainly varies somewhat from the zonal mean, since otherwise its thermal wind balance could not support the anomalous local temperature variation observed by Orton et al. (1998). Although the comprehensive modeling of the hot spot circulation is beyond the scope of this paper, Appendix C outlines simple quantitative estimates plausibly accounting for the compatible differ-

ence between the Galileo Doppler wind shears and the zonal mean flow modeled in Fig. 6.

As pointed out by Williams (1997), the close agreement between the Galileo Doppler wind speed and that for angular-momentum conserving flow at the entry latitude, as circulated from some vanishing velocity level over the equator, seems "almost too close to be coincidental". For a specific angular momentum $M \equiv a\cos\lambda(U+\Omega a\cos\lambda)$ equal to its value at the equator, $U_m = \Omega a \sin^2\lambda/\cos\lambda$. As evaluated with Ωa = 12,568 m s^{-1} for Jupiter at latitudes of 6–7°, for example, $U_m \approx$ 138–188 m s^{-1}, as compared with the Doppler measured speed of about 170 m s^{-1} (Atkinson et al., 1998). This "coincident" feature of the Doppler wind measurement appears to be in consonance with the constructed thermocline section for Jupiter. Fig. 6 shows as heavy dashed curves contours of specific angular momentum intersecting the 3 bar level at 4, 6, 8, and 10° latitude. As anticipated by Allison et al. (1995), the modeled angular momentum surfaces are approximately parallel at upper levels to the potential temperature surfaces, as for a nearly vanishing Ertel PV in the equatorial region (cf Allison et al., 1994), and the constant-M surface intersecting the upper level flow at 6° latitude is rooted down to deep levels on the equator a short distance above the bottom of the flow layer. Although "angular momentum conserving flow" is typically associated with an axially symmetric regime

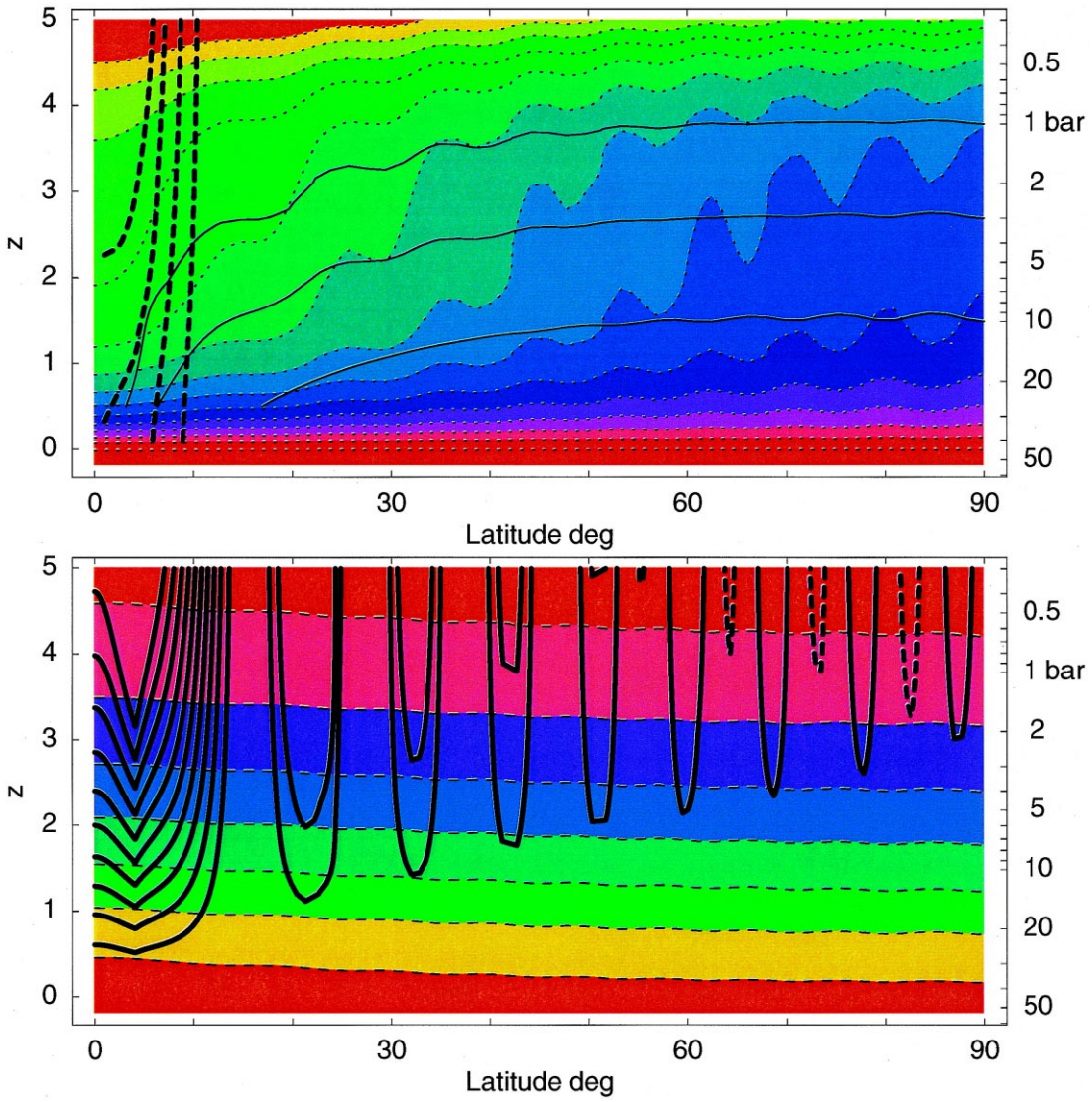

Fig. 6. Thermocline section for the Jupiter model with $p_0 = 44$ bar. Upper portion (a) shows potential temperature as short-dashed, color-filled contours increasing upward in 10 K increments. Heavy dashed curves show contours of specific angular momentum intersecting the 3 bar level at 4, 6, 8, and 10° latitude. The thin solid lines show constant surfaces of (the downward increasing) PV field intersecting the pole at 1, 3, and 10 bars. Lower portion (b) shows the kinetic temperature as dashed, color-filled contours decreasing upward in 20 K increments. Solid curves show the westerly flow contoured at intervals of 20 m/s.

(e.g. Held and Hou, 1980), the maintenance of the local maximum of specific angular momentum over the equator requires some "up-gradient" eddy transport, as discussed by Hide (1969) and Read (1986b). While the adopted PV recipe for the modeled Jupiter thermocline avoids any specific assignment of the relative roles of eddies and symmetric mean flow in this region, the exposed link between the Doppler wind measurement and the deep equatorial level may suggest an important constraint on the meridional–vertical structure of explicit three-dimensional models for the maintenance of the equatorial jet. The constant angular momentum surfaces are also approximately parallel to the potential temperature surfaces shown for the modeled Saturn thermocline in Fig. 7. In this case, however, the constant-M surface intersecting the peak equatorial velocity at upper levels is rooted down to a relatively higher level above the equator where the wind is already built up to nearly half its strength aloft, consistent with the larger potential temperature contrast and the stronger equatorial jet speed. It may be of some interest that the illustrated potential temperature surfaces appear to offer a connection between the lowest half-scale height of the wind layer at all latitudes and upper levels approaching the emission layer at the pole. Could these be the conduits for the upward-poleward redistribution of the internal heat flux of both planets? Although the level of no motion is by construction coincident with the $z^*=0$ level, it is also of some interest that the modeled sections for

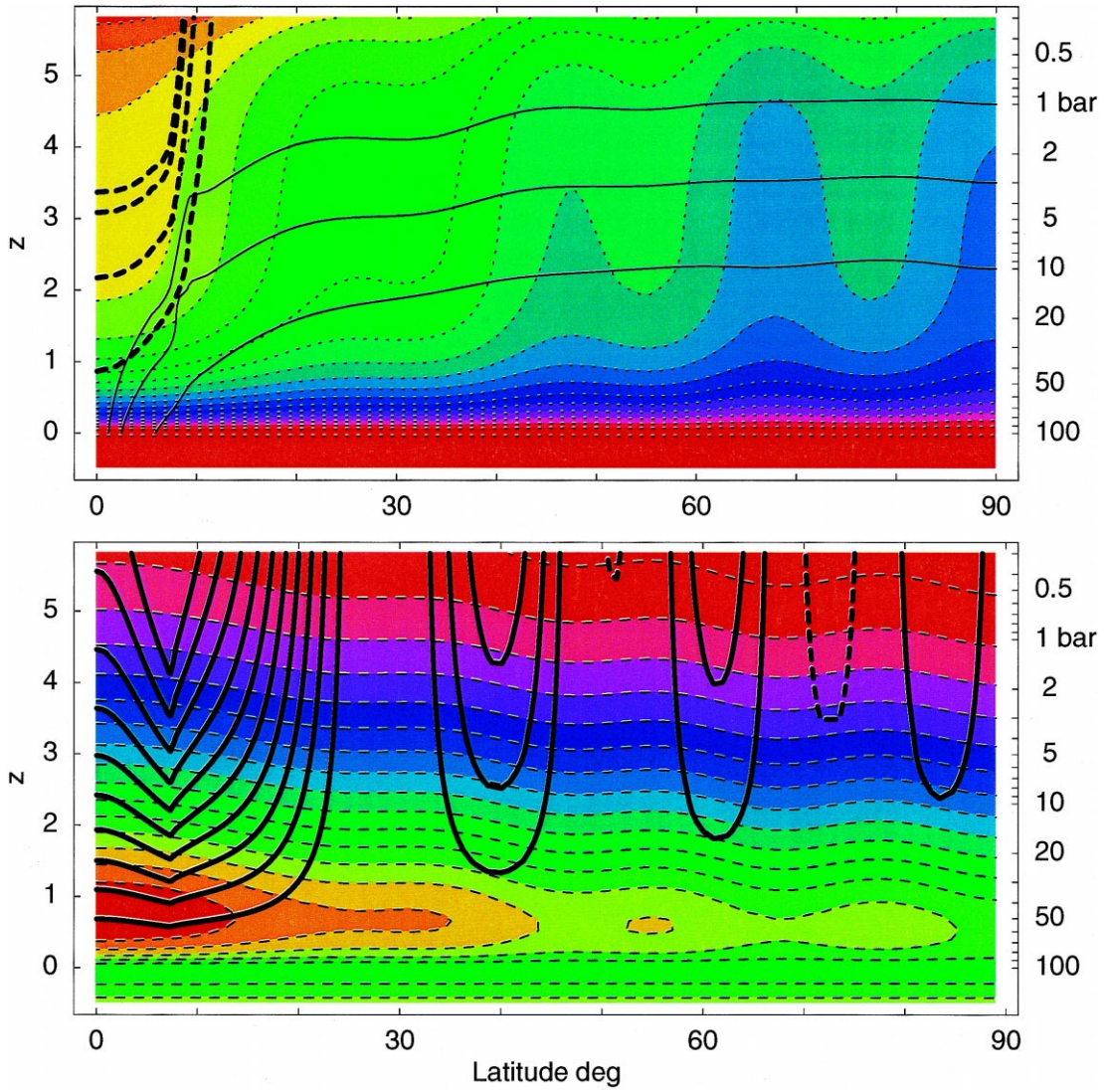

Fig. 7. Thermocline section for the Saturn model with $p_0=100$ bar. Upper portion (a) shows potential temperature as short-dashed, color-filled contours increasing upward in 20 K increments. Heavy dashed curves show contours of specific angular momentum intersecting the 3 bar level at 4, 6, 8, and 10° latitude. The thin solid lines show constant surfaces of (the downward increasing) PV field intersecting the pole at 1, 3, and 10 bars. Lower portion (b) shows the kinetic temperature as dashed, color-filled contours decreasing upward in 20 K increments. Solid curves show the westerly flow contoured at intervals of 50 m/s. (A high-latitude 50 m/s easterly contour is also shown dashed.)

both planets show a poleward-upward displacement of the lowest contoured isotachs for the predominantly westerly flow.

5. Perspective

On the opening day of the symposium in Nantes where this paper was presented orally, Dr Daniel Gautier reminded the assembled participants that we were meeting in the home city of Jules Verne (1828–1905). Finding his material in the geophysics, astronomy, and mechanics of his day, Verne's devotion to the "facts" then at hand is renowned. His account of a lunar voyage includes a review of the equations of orbital astronautics and from the seagoing Nautilus he provides enough information about the width and depth and speed of the Gulf Stream for an estimation of its thermal current balance and vorticity. But in his storied excursion to Jupiter (1877, *Off on a Comet*), Verne anticipated the outstanding puzzle of the cloud bands even as they might be observed from a distance of only 43 million miles, remarking that "the physiology of belts and spots alike was beyond the astronomer's power to ascertain ..."

Knox and Croft (1997) have discussed the value of "storytelling" in the education of meteorologists, and emphasize among several vivid examples the concept of PV, suggesting that "PV thinking allows one to look beyond the myriad details of the dynamical evolution of the flow and skip to the end ..." (of the story). This paper attempts to present a particular "story" for the jovian dynamics, assuming an internal entropy contrast for a dynamic weather layer plausibly consistent with the Galileo probe measurements and accumulated wave diagnostics, along with a smoothly stirred variation of PV for the associated "thermocline". Although mathematically idealized, the intention is to provide a quantitatively explicit account of the Jupiter wind currents, specifically simple and concrete enough to suggest its refutation or useful qualification with new missions and measurements.

The reference to the hypothesized latitude–height structure as a "thermocline" stands in a long line of comparisons of the jovian dynamics to the oceanic circulation (e.g. Williams, 1975). Its usage for the giant planets was anticipated by Arthur Clarke's imaginative but remarkably prescient (1973) story of Jupiter's equatorial cloud zone, and the oceanic density structure seems to offer an especially pertinent parallel to the proposed variation of potential temperature in the jovian troposphere. As described by Pedlosky (1996), the (oceanic) "... density field in fact varies so strongly that the overall *horizontal* variation in density is as large as the overall *vertical* variation in density in each of the gyres. This implies that an explanation of the observed density field requires, at a minimum, a relaxation of the quasi-geostrophic approximation ... Moreover, we anticipate that the horizontal and vertical structures are linked through the motion field. This is the problem of the thermocline". As with the oceanic currents and gyres, the parametric representation of the PV distribution on Jupiter may present an insightful approach to the modeling of the interdependent temperature–velocity structure.

Stommel's (1954, 1955) inertial model for the western intensification of the oceanic Gulf Stream is a vivid antecedent to this way of thinking. Defining a thickness of water h between the 17 and 19°C isotherms of the upper Stream, Stommel noted that since the relative vorticity of the Sargasso Sea (toward the open ocean) nearly vanishes, the cross-stream conservation of potential vorticity may be expressed as $(f+\partial v/\partial x)=f(h/h_0)$, where h_0 is the vertical distance between the isothermal surfaces in the stagnant waters to the east. The charted current speed derived from the integrated vorticity, $v(x)=\int_\infty f(h/h_0-1)\mathrm{d}x$, shows a remarkable agreement with the geostrophic velocity as directly computed from the thickness variation and suggests that the width of the Stream may be controlled more by purely inertial effects than by eddy viscosity. The coupled constraints of geostrophic balance and PV conservation can be expressed as a simple relation for the exponential eastward drop of the northward flow from its western maximum over a horizontal deformation scale, related to the baroclinic stratification, also given as $L_\mathrm{D}=V_\mathrm{max}/f$. Stommel's simple idea has figured in many later refinements of ocean current theory (e.g. Huang and Stommel, 1990), and was the original inspiration for the present study of Jupiter.

Jupiter, like the Earth, is a rapidly rotating planet for which the potential temperature (Θ) variations associated with colder-poleward regions of the atmosphere are balanced by the Coriolis acceleration of vertical (thermal wind) shear toward upward-stronger, west-to-east flow. While the *kinetic* temperature decreases upward within the tropospheres of both planets, the accounted compressibility adjustment of the defined *potential* temperature implies its *upward increase* everywhere within their statically stable wind layers, as for oceanic temperature. Unlike the Earth's atmosphere, however, where horizontal gradients are strongly loaded on to the ground, Jupiter has no rigid lower surface. As an adiabatically conserved variable, directly related to the entropy, Θ is homogenized by convection, and on Jupiter, the deep internal convection maintains a vanishing horizontal Θ gradient at the bottom of its wind layer, coincident with the lowest level of a region of concentrated, upward-decreasing static stability.

The deep stable region may be imposed by some

microphysical–dynamical adjustment of condensed water or by a deeply embedded layer of efficient radiative transport, consistent with the diagnostic indications of equatorial wave dispersion and associated stratospheric propagation, the slow westward drift (with respect to System III) of Jupiter's Great Red Spot, the shock-front analysis of the SL9 impacts at Jupiter's mid-latitudes, and most recently the direct *in-situ* measurement of downward-increasing stability (and water abundance) from the Galileo entry probe.

Gradients of wind and temperature above the bottom of the wind layer within the jovian "thermocline" imply a direct correlation of horizontally warmer Θ with more vertically layered Θ. This warmer–stabler correlation is just the reverse of that on the Earth where colder-poleward latitudes are more statically stable. The difference between the two planets is again a direct consequence of their very different lower boundaries and stratifications. While the Earth's atmosphere exhibits a "top-down" unpacking of Θ surfaces, nearly flat at the tropopause, but strongly graded at the surface (cf Fig. 1), Jupiter unpacks its Θ surfaces from the bottom-up, flat at the bottom of the wind layer, but nearly vertical toward the top, as scaled by the vertical-to-horizontal aspect ratio (cf Fig. 2), and the near-vertical slope of Θ surfaces within the upper wind layer implies a self-similar link of vertical shear to the wind itself at each level (by the therefore separable vertical integration of the thermal wind equation). The resulting "jovistrophic" balance means that Θ surfaces are sloped upward/downward toward the pole in direct proportion to the strength of the westerly/easterly flow, as weighted by the sine of the local latitude (zero at the equator and one at the pole).

The jovistrophic wind balance may be numerically calibrated in terms of an associated "deformation scale" (L_D), defined in proportion to the square root of the product of the gas constant and the vertical Θ contrast at the pole, divided by twice the planetary rotation frequency, but scaled by a roughly order one factor depending weakly on the uncertain depth of the flow layer. Although the as yet unobserved flow depth and the full Θ contrast cannot be uniquely selected from among a physically plausible range of tradeoffs of one against the other, the L_D parameter is itself uniquely related to the latitudinal flow profile at some evaluated level. The jovistrophic scaling velocity is just the square of L_D times the equatorial "beta parameter" (itself twice the planetary rotation frequency divided by the planetary radius).

The layered packing of Θ surfaces in the atmosphere also represents a reservoir of vorticity. The "relative vorticity" is the negative latitudinal shear of the flow, by definition cyclonic wherever the winds are more strongly east-to-west (or easterly) in the poleward direction, and anticyclonic wherever more strongly westerly-poleward. The "planetary vorticity" or "Coriolis parameter" is just twice the planetary rotation frequency times the sine of the local latitude, and the sum of the relative plus planetary vorticity is commonly referred to as the "absolute vorticity". The *potential vorticity* or PV is essentially the product of the static stability and the absolute vorticity.

The at first seemingly obscure concept of PV visualization repays its studied engagement with a simple geometrical portrayal of complex dynamical balances. Although the dynamically equilibrated state is presumably determined by competing budgets for both upward and poleward transports of momentum and potential energy, both by eddies and mean-meridional circulations, the available observations, numerical modeling, and theoretical stability studies suggest that the accumulated effect of these may be generally characterized by approximately monotonic and locally/globally smoothed PV distributions. (A change in the sign of the PV or its latitudinal gradient within each hemisphere, for example, are well-known flags for dynamical instabilities, typically resulting in a PV readjustment to something near its marginally neutral state.) On the Earth, the observations plotted in Fig. 1 show a positive-poleward PV gradient concentrated in the vicinity of the "sub-tropical" jet, with relatively slow variations at both lower and higher latitudes. The strength of the terrestrial flow itself corresponds to the thermal wind balance of a dynamically mediated reduction in the radiatively forced equator-to-pole Θ contrast that would exist in the absence of motions, consistent with a nearly monotonic poleward PV.

Although the PV distribution within Jupiter's deep thermocline is as yet unobserved, it too may be expected to vary almost monotonically over latitude from zero at the equator toward its polar value, but with some local variation in step with local changes in relative plus planetary vorticity and temperature. Anticipating an overall decrease in Θ from equator-to-pole for the "jovistrophic" balance of the strong equatorial jet and predominantly west-to-east circulation, suppose the PV varies over latitude as the normalized deficit of the squared horizontal Θ contrast, as measured with respect to its polar value. This would imply a vanishing PV at the equator (where the deficit of the squared Θ contrast is small) and a disproportionate, nearly level smoothing toward high latitudes (where the deficit for a small relative Θ difference changes slowly with respect to its polar value). The same recipe provides a good fit to the equator-to-pole variation of PV at 200 mb in the Earth's atmosphere, as shown in Fig. 1. But for the assumed jovian thermocline, the relative latitudinal Θ contrast is the same as the latitudinally variable augmentation of the static stability with respect to its value at the pole. For Jupi-

ter, the PV recipe therefore specifies a deficit for the relative Θ contrast equal to the normalized absolute vorticity.

Again, the "jovistrophic" balance of the tropospheric circulation implies an upward-poleward (or downward-poleward) deformation of Θ surfaces for westerly (or easterly) flow, as for colder-poleward (or warmer-poleward) temperatures; while the correlated PV distribution specifies a normalized absolute (relative plus planetary) vorticity given as the deficit (or one minus) the relative Θ contrast. Now away from the equator, poleward of the "horns" of the equatorial jet, the planetary vorticity dominates the absolute vorticity, and the overall decrease of planetary vorticity from high to low latitudes implies a decrease in the Θ deficit and, therefore, a compensated increase in warmer temperatures there. The jovistrophic balance of warmer temperatures toward lower latitudes corresponds to an equatorial intensification of west-to-east flow, as in the cyclonic flanks of the equatorial jet. The effect is analogous to Stommel's inertial model for the westward intensification of the faster–thinner flow of the Gulf Stream, but controlled by the latitudinal variation of the Coriolis parameter, as well as the layered Θ.

Within the horns of the equatorial jet, the Θ contrast is very nearly unity, and the absolute vorticity is nearly zero, as for an anticyclonic flow shear equal to the equatorial planetary vorticity. But on sub-planetary scales away from the equator, comparable to the spacing of the mid-latitude jets, the *latitudinal variation* of the absolute vorticity is dominated by the *latitudinal variation* of the relative vorticity (or latitudinal flow curvature). This means that latitudinal changes in the horizontal shear of the jets correspond to latitudinal changes in static stability and Θ (in the sense that more-cyclonic poleward regions are also cooler-poleward), and the associated jovistrophic correlation of temperatures with the flow velocity implies an alternation of the flow direction over latitudinal scales comparable to L_D. West-to-east flow near the pole, for example, implies a jet curvature extending to east-to-west flow in the equatorial direction implying a jet curvature extending to west-to-east flow implying ... a successive, ever-after alternation down to the equatorial jet.

Acknowledgements

I wish to thank Christophe Sotin and the other organizers of the Nantes Symposium for hosting such an important and pleasant meeting. I am grateful to Anthony Del Genio, Ru Xin Huang, Lorenzo Polvani, Peter Read, and Larry Travis for their advice and encouragement with this work, which was supported by the NASA Planetary Atmospheres Program under the management of Jay T. Bergstralh.

Appendix A. Potential vorticity, gradient balance, and the jovian regime

As formulated by the conservation theorem of Ertel (1942), the PV may be defined as $q \equiv \rho^{-1}\zeta_a \cdot \nabla\Theta$, where ρ is the density and $\zeta_a \equiv \nabla \times (\mathbf{U} + \Omega \times \mathbf{r})$ the vector absolute vorticity, with $\mathbf{U}$ the vector velocity relative to the planetary rotation velocity $\Omega \times \mathbf{r}$. For zonal-mean motion in a baroclinic, but vertically hydrostatic atmosphere on a sphere of radius a, using the log-pressure coordinate $z^* = \ln(p_0/p)$ to measure elevation in scale heights ($H = RT/g$) above the reference pressure p_0, the Ertel PV

$$q = (g/p_0)e^{z^*}\left[\frac{\partial U}{\partial z^*}\frac{\partial\Theta}{a\partial\lambda} + (\zeta + f)\frac{\partial\Theta}{\partial z^*}\right] \tag{A1}$$

(cf Stevens, 1983). Here g is the gravitational acceleration, U the zonal mean velocity, $\zeta \equiv -(a\cos\lambda)^{-1}\partial(U\cos\lambda)/\partial\lambda$ the zonal-mean relative vorticity on a sphere of radius a and $f = 2\Omega\sin\lambda$ the vertical component of planetary vorticity or Coriolis parameter at latitude λ. To the extent that the relative vorticity can be evaluated on a constant-Θ surface (as ζ_Θ), this is equivalent to $q = (g/p_0)e^{z^*}(\zeta_\Theta + f)\partial\Theta/\partial z^*$, as sometimes used in terrestrial weather maps (cf Hoskins et al., 1985).

The Ertel PV should not be confused with the shallow water PV, $q_{SW} = (\zeta + f)/D$, assuming a discrete layer of constant density fluid of variable thickness D, or with any of several forms of the quasi-geostrophic (or "pseudo") PV, e.g. $q_{QG} = f_0 + \beta y + \zeta + f_0\, e^{z^*}\partial_{z^*}[e^{-z^*}\theta(\partial_{z^*}\Theta)^{-1}]$, as restricted to sub-planetary scale domains and with an assumed horizontally uniform static stability ($\partial\Theta/\partial z^*$) or mean thickness parameter. Although $dq_{QG}/dt = 0$ can, under certain special circumstances, represent an appropriate approximation to the conservation statement $dq/dt = 0$, q_{QG} itself is *not* an approximation to the Ertel PV, as noted in the Appendix of the book by Hoskins and Pearce (1983).

Now for gradient-balanced, zonal-mean motion on the sphere

$$(1 + U/\Omega a\cos\lambda)f\partial U/\partial z^* = -R\partial T/a\partial\lambda \tag{A2}$$

and the PV as given by (A1) can be expressed as

$$q = \frac{g\, e^{z^*}}{p_0}\left[(\zeta + f) - \frac{2\tan\lambda}{a\ Ri}(U + \Omega a\cos\lambda)\right]\frac{\partial\Theta}{\partial z^*} \tag{A3}$$

where

$$Ri \equiv \frac{R \cdot \mathrm{e}^{-\kappa z^*} \partial\Theta/\partial z^*}{(\partial U/\partial z^*)^2} \equiv \frac{\Gamma}{(\partial U/\partial z^*)^2} \tag{A4}$$

is the Richardson number, equivalent to the squared ratio of the Brunt–Vaisäla frequency to the vertical wind shear. Expanding the metrical form of the relative vorticity on the sphere, $\zeta \equiv -(a\cos\lambda)^{-1}\partial(U\cos\lambda)/\partial\lambda = -\partial U/a\partial\lambda + U\tan\lambda/a$, (A3) can be rearranged with grouped factors of Ri and $Ro_G \equiv U/\Omega a\cos\lambda$ as

$$q \equiv \frac{g\,\mathrm{e}^{z^*}}{p_0}\left[-\frac{\partial U}{a\partial\lambda} + f - \frac{f}{Ri}\left(1 + \frac{U}{\Omega a\cos\lambda} - \frac{U}{2\Omega a\cos\lambda}Ri\right)\right]\frac{\partial\Theta}{\partial z^*}. \tag{A5}$$

Then for $Ro_G \le 1$, but arbitrary Ri (the terrestrial geostrophic regime), $q_{geo} = (g/p_0)\mathrm{e}^{z^*}[-\partial U/a\partial\lambda + U\tan\lambda/a + f(1 - Ri^{-1})]\partial\Theta/\partial z^*$, the same as Eq. (6.2) of Hitchman and Leovy (1986), and since under typical terrestrial conditions, $Ri \ge Ro_G^{-1}$, the familiar form of $q \approx \rho^{-1}(\zeta + f)\partial\Theta/\partial z^*$ is a good approximation to the Ertel PV for this parameter setting.

On the jovian planets, however, where Ro_G is generally even smaller than on the Earth, it appears likely that $Ri < Ro_G^{-1}$, as previously proposed by Gierasch (1976). At the cloud-tracked wind level, $Ro_G^{-1} \equiv \Omega a\cos\lambda/U$ is about 70 for Jupiter's equatorial jet or 20 for Saturn's. Inertial stability demands that $q/f \ge 0$ (cf Stevens, 1983) and, as noted by Allison et al. (1995), a fit of the cloud-tracked wind profiles for Jupiter and Saturn to plausibly small variations in the PV within their equatorial jets suggests that $Ri \sim 2$–3 there. At higher latitudes, weaker winds would imply larger values for Ri (assuming a static stability decreasing less rapidly than the squared vertical wind shear), but also larger values for Ro_G^{-1}. Then assuming a realization of the parameter setting $Ro_G < 1/Ri \ll 1$, (A5) reduces to the especially simple form

$$q_{jovi} \approx \frac{g\,\mathrm{e}^{z^*}}{p_0}\left[-\frac{\partial U}{a\partial\lambda} + f\right]\frac{\partial\Theta}{\partial z^*}. \tag{A6}$$

The more essential distinguishing feature of the jovian regime is its implied small ratio of vertical-to-horizontal potential temperature gradients (as scaled by the vertical-to-horizontal aspect ratio of the atmosphere), as discussed by Gierasch (1976) and Allison et al. (1995). This means that the latitudinal PV gradient will depend importantly on the horizontal variation of the static stability, as implied by the assumed potential temperature structure given by Eq. (1). Then for $\partial\Theta/\partial z^* \equiv \mathrm{e}^{\kappa z^*}\Gamma/R$ and a static stability index given by Eq. (1b) as $\Gamma = \Gamma_0(1 + \theta/\Delta\theta)\mathrm{e}^{-(1/\delta+\kappa)z^*}$, with $\Gamma_0 \equiv (R\Delta\theta/\delta)$, the PV of the jovian thermocline becomes

$$q_{jovi} \equiv \left(\frac{g\Delta\theta}{\delta p_0}\right)\mathrm{e}^{(1-1/\delta)z^*}\left[-\frac{\partial U}{a\partial\lambda} + f\right]\left(1 + \frac{\theta}{\Delta\theta}\right). \tag{A7}$$

Then specifying q_J in terms of a normalized function $\Pi(\lambda, z^*) \equiv q(\lambda, z^*)/q_p(z^*)$, expressing its ratio to its polar value q_p at the same level, the latitudinal "PV balance" for the deep jovian troposphere reads

$$(f - a^{-1}\partial_\lambda U)(1 + \theta/\Delta\theta) \equiv 2\Omega(1 + \varepsilon)\Pi(\lambda, z^*) \tag{A8}$$

where ε denotes the ratio of the relative to planetary vorticity at the pole. This neglects the augmentation of the static stability within the radiative topping layer aloft, as appropriate for pressures greater than 2 bar. Π is by definition unity at the pole and, excluding some equatorial asymmetry, necessarily zero at the equator. Eq. (A8) is by itself simply a normalized representation of the Ertel PV for the assumed jovian thermocline. Its essential novel feature is its representation of the fully variable static stability in terms of the horizontal potential temperature contrast of the assumed jovian wind layer.

Appendix B. Analytic waveguides and inferred static stability for the deep jovian troposphere

Allison (1990) proposed a simple model for the ducting of waves in Jupiter's equatorial atmosphere, intended to provide a coherent account of apparent vertical oscillations in the Voyager radio occultation retrievals of stratospheric temperatures (Lindal et al., 1981), as well as their assumed correspondence with imaging and infrared observations of the equatorial plumes (e.g. Hunt et al., 1981). Modeling a leaky waveguide with a sandwiched, piecewise-constant static stability Γ_0 of thickness d (scale-heights) overlying an adiabatic interior and surmounted by a weakly stable troposphere aloft, the analytic approximation to the numerically evaluated eigenvalue problem implied a gravest "equivalent depth" h_0 with

$$(gh_0)^{1/2} \approx (d\,\Gamma_0)^{1/2} \tag{B1}$$

where g is the gravitational acceleration.

Ingersoll et al. (1994) proposed a similar tropospheric waveguide for the ducting of anticipated wave fronts generated by the SL9 impacts on Jupiter, but assuming a more realistic continuous variation of the deep-seated stability equivalent to $\Gamma_0 \exp[-(1/\delta + \kappa)z^*] = \Gamma_0 \exp(-2z^*)$, with the result that

$$(gh_0)^{1/2} \approx (2/\pi)\Gamma_0^{1/2}. \tag{B2}$$

This would therefore be comparable to the model proposed by Allison (1990) for a stable layer thickness $d \approx (2/\pi)^2 \approx 0.4$. Ingersoll and Kanamori

(1995) and Hammel et al. (1995) applied the exponential waveguide model to the observed expansion of the SL9 shock fronts, interpreted as deeply ducted gravity waves. With $c_e=(gh_0)^{1/2} \approx 450$ m s^{-1}, $(NH)_0=\Gamma_0^{1/2}\approx 707$ m s^{-1}, as indicated for comparison with the modeled stability profile shown in Fig. 3. This idealized model, corresponding to NH varying inversely with the pressure depth, is the same as the vertical structure implied by Eq. (1b) for the assumed jovian thermocline template with an e-folding scale $\delta=(2-\kappa)^{-1} \approx 0.59$. As discussed by Allison and Atkinson (1998), a deep region of downward increasing stability of the same form is suggested by the apparent long-period variation of the Galileo probe Doppler frequency residuals at levels between 2 and 20 bars over roughly even pressure intervals (cf Fig. 7 of Atkinson et al., 1998), interpreted as small-scale gravity waves.

Allison (1990) suggested that $h_0 \approx 1$–5 km provided a reasonable match to the apparent stratospheric wavelengths in the Voyager radio data, as well as plausible constraints on the horizontal dispersion properties and equatorial trapping distance of the plumes, interpreted as equatorial Rossby waves drifting to the west with respect to the mean zonal flow at some 50 m s^{-1}. More recently, Ortiz et al. (1997) have provided a convincing corroboration of a wave phase drift of 40–50 m s^{-1} for equatorial thermal features in the vicinity of the 2 bar level on Jupiter, based on a time series analysis of 5 μm features tracked over three years at the Infrared Telescope Facility. Then for the inferred range of equivalent depths (B2) would imply $(NH)_0 \leq$ 530 m s^{-1}, somewhat less than the result of Ingersoll and Kanamori (1995) for the mid-latitude region of the SL9 impacts. As noted, however, by Ortiz et al., the neglect of vertical shear in the wave diagnosis by Allison (1990), along with uncertainties in the mean zonal flow at the sounding level, could imply an underestimate of h_0 (and therefore the static stability at deeper levels), as suggested by a simple Doppler-shifted adjustment of the linear dispersion relation. The same problems would also apply to the L_R scale adopted by Williams and Wilson (1988), as evaluated for the observed relative westward drift of jovian vortices.

The diagnosis of the SL9 impacts by Ingersoll and Kanamori (1995) is much less susceptible to the uncertain effects of mean flow and wind shear, owing to the much larger phase speeds of the interpreted gravity waves and may for this reason be regarded as a more reliable calibration of the deep static stability on Jupiter. The SL9 result is also an important indication of deep static stability extended to mid-latitudes.

If the static stabilization is maintained by condensation processes, the vertical e-folding scale δ for the potential temperature variation at deep levels could be less than ~0.2 pressure scale heights (cf Barcilon and Gierasch, 1970; Acterberg and Ingersoll, 1989; Del Genio and McGrattan, 1990), implying a possibly large offset of the temperature from the deep adiabat. Although the actual deep stability structure may therefore have a different vertical scale than for the idealized model ($\delta \approx 0.59$ in the notation used here), Ingersoll et al. (1994) indicate that its resonant response function is similar to that numerically calculated by Acterberg and Ingersoll (1989) for a moist adiabat with a slightly larger $(NH)_0$ value, a slightly smaller pressure depth, and an e-folding scale for the associated potential temperature gradient roughly equivalent to $\delta \sim 0.16$.

If the stable structure is maintained by a deep radiative layer, its vertical scale could be ~1 or larger (cf Figs. 5 and 6 of Guillot et al., 1994). Although the real situation is as yet poorly constrained by the observations, the waveguide interpretation requires a deep but vertically isolated stable region, with δ small compared to the total thickness z_T^* for the tropospheric wind layer. While there are no available analytic solutions to the equivalent depth for an exponential waveguide with an arbitrary e-folding scale, the comparison of (B2) with the result (B1) for a sandwiched piecewise constant stability model suggests that $(NH)_0$ may scale roughly with $(0.6/\delta)^{1/2}$.

Appendix C. Galileo probe winds versus the zonal mean flow

If, as pointed out by Showman and Ingersoll (1998), the probe descended within the periphery of a local vortex, then the interpretation of the Doppler measurement could involve a large centripetal modification to the zonal thermal wind balance. They also point out that both the Doppler and probe accelerometry retrievals assume perfect zonality and could, therefore, bear the sensitive convolution of meridional motions. Showman and Ingersoll (1998) favor an anticyclonic interpretation of the probe descent region, as for a gradient wind balance with a negative radius of curvature $r_c \approx -4000$ km, and a corresponding locally warmer-poleward temperature gradient. Their interpretation affords a possible account of how the probe site could be warmer than the equatorial region to the south and, therefore, of a lesser local density at deep levels perhaps suppressing the rise of moist plumes from below.

If, however, the 5 μm "hot spot" where the probe entered the atmosphere really corresponds to emission from a deeper cloud-free region, actually both cool and cyclonic with respect to its surroundings at the same level below the cloud deck (as described for similar features by Conrath et al., 1981), then the relevant radius of curvature would be positive. (This would

also be consistent with the adopted PV-Θ parameterization implying a correlation of cooler regions with cyclonic shear.) To the extent that the probe Doppler winds are at least comparable to the actual zonal mean flow, and that this is geostrophically balanced as assumed for the modeled jovian thermocline, the local latitudinal gradient of temperature at the probe site must represent only a small departure from the zonal mean gradient at the same latitude and level. Then by a comparative application of the separate thermal wind shear equations for the zonal mean and the local gradient flows, as expressed by Eqs. (4) and (6) of Showman and Ingersoll (1998), $\partial U_{\rm zonal}/\partial z^* \approx (1 + 2U_{\rm probe}/r_c f_0)\partial U_{\rm probe}/\partial z^*$. With $f_0 \approx 4 \times 10^{-5}$ s^{-1} at the probe entry latitude, $U_{\rm probe} \approx 170$ m s^{-1} as measured by the Doppler wind experiment, and taking $r_c \approx +4000$ km, the implied zonal mean vertical shear $\partial U_{\rm zonal}/\partial z^* \approx 3 \times \partial U_{\rm probe}/\partial z^*$, more nearly consistent with the indication of the modeled isotachs shown in Fig. 6. If r_c were as small as implied by the roughly 1° or 1200 km (2 pixel) latitudinal span of the bright center shown in Plate 3 of Orton et al. (1998), the probe vertical shear would be about 1/10 that of the zonal mean flow.

If the modeled thermocline turns out to be qualitatively correct, then presumably the strength of the swirl at the probe entry site would have to be rapidly diminished somewhere below 20 bar toward deeper levels coincident with the bottom of the wind layer, where the local temperature gradient of the vortex would necessarily be very different from that of the zonal mean shown in Fig. 6. The implied strong gradients and shear near the bottom of the cyclone could be supported, however, by the relatively strong static stability consistent with the assumed vertical structure. The only firm limit would be the inertial stability of the axisymmetric vortex, requiring a Richardson number $Ri > 1$, with $\partial U/\partial z^* = NH/Ri^{1/2}$. Assuming the static stability at the bottom is as large as that inferred by Ingersoll and Kanamori (1995) from the SL9 impacts, with $(NH)_0 \approx 700$ m s^{-1} (see Appendix B), but with Ri as large as four in the vortex, for example, the vertical shear could be as large as $\partial U/\partial z^* \approx 350$ m s^{-1}, admitting a build-up to the Doppler wind speeds within a layer above the bottom of the flow layer as thin as $U_{\rm probe}(\partial U/\partial z^*)^{-1} \approx 170/350$ m s^{-1} ≈ 0.5 scale height.

Assuming the deep vortex has a temperature structure of the same form as specified by Eq. (1), $\partial_r T = e^{-\kappa z^*}(1 - e^{-z^*/\delta})\partial_r \theta \approx \partial_r \theta$, for $\delta \ll z^* < 1$, and by vertical integration of the gradient thermal wind equation, its radial temperature depression would be given as $Rz^* \partial_r T \approx (V^2/r_c + f_0 V)$, where V is the swirl speed. Although the radial distribution of the swirl is itself apparently unknown, suppose this varies inversely with distance from its center, beyond the estimated radius of curvature r_c, with $V_{\rm swirl} \approx U_{\rm probe}(r_c/r)$. This would be consistent with a reduction of the angular velocity of the swirl to 1/2 the local planetary vorticity f_0 at a radial distance $r_0 \approx (2U_{\rm probe} r_c/f_0)^{1/2}$ and a corresponding "compactness" $r_0/r_c \approx (2U_{\rm probe}/r_c f_0)^{1/2}$ in the range of 4–2 for $r_c \approx 500$–2000 km. Then for $r_c < U_{\rm probe}/f_0 \approx 4000$ km, $U^2_{\rm probe} r_c^2/r^3 \approx Rz^* \partial T/\partial r$, and upon integration from r_c to the far field (at $r \approx r_0 \gg r_c$), the radial temperature contrast for the local vortex would be $\Delta_r T \approx U^2_{\rm probe}/2Rz^*$, approximately independent of r_c. With a rooted shear zone for the vortex as small as $z^* \approx 0.5$, this would imply $\Delta_r T \approx 8$ K (cooler) at deep levels, as realized at a pressure in the vicinity of 17 bar, as indicated in Table 1. As diminished with height by a factor $(p/p_0)^\kappa$, as for a modeled thermocline with a bottom pressure of 30–50 bar, the corresponding local thermal depression at the 1 bar level would amount to no more than 2–3 K. This compares favorably with the slightly cooler temperatures observed by the Atmospheric Structure Instrument (ASI), as these differ from remote sensing measurements, and consistent with their interpretation by Orton et al. (1998) that this is "probably because the low-temperature ASI features are confined to regions smaller than the ~6000-km resolution of the remote sensing".

While these estimates are only the barest sketch of a coherent model of the interpreted "hot spot" circulation, greatly simplifying the probable nonlinear vortex-mean flow dynamics, they suggest that the vertical structure of the zonal mean wind for the modeled Jupiter thermocline may be roughly consistent with the Galileo Doppler data. Alternatively, dynamically similar but much deeper thermocline models could be constructed with weaker vertical shears above the 20 bar level, for a depth of vanishing motion extending well below the specific examples constructed for illustration, perhaps down to several hundreds of bars. Williams (1997), for example, has performed numerical simulations of planetary vortices with a baroclinic Jupiter model with assumed zonal winds fitted at the top to the Galileo Doppler data, but approaching a level of no motion at represented depths some 400 km below.

References

Acterberg, R.K., Ingersoll, A.P., 1989. A normal-mode approach to Jovian atmospheric dynamics. J. Atmos. Sci. 46, 2448–2462.

Allison, M., 1990. Planetary waves in Jupiter's equatorial atmosphere. Icarus 83, 282–307.

Allison, M., Del Genio, A.D., Zhou, W., 1994. Zero potential vorticity envelopes for the zonal-mean velocity of the Venus/Titan atmospheres. J. Atmos. Sci. 51, 694–702.

Allison, M., Del Genio, A.D., Zhou, W., 1995. Richardson number constraints for the Jupiter and outer planet wind regime. Geophys. Res. Lett. 22, 2957–2960.

Allison, M., Atkinson, D.H., 1998. A wave-dynamical interpretation of Doppler frequency residuals from the Galileo atmospheric entry probe. The Jovian System after Galileo — The Saturnian System before Cassini–Huygens — Abstracts. Nantes Cedex, France: Laboratoire de Géophysique et Planétologie. p. 9.

Atkinson, D.H., Pollack, J.B., Seiff, A., 1998. The Galileo probe Doppler wind experiment: measurement of the deep zonal winds on Jupiter. J. Geophys. Res. 103, 22,911–22,928.

Banfield, D., Gierasch, P.J., Bell, M., Ustinov, E., Ingersoll, A.P., Vasavada, A.R., West, R.A., Belton, M.J.S., 1998. Jupiter's cloud structure from Galileo imaging data. Icarus 135, 230–250.

Barcilon, A., Gierasch, P., 1970. A moist, Hadley cell model for Jupiter's cloud bands. J. Atmos. Sci. 27, 550–560.

Barnes, J.R., Haberle, R.M., 1996. The martian zonal-mean circulation: angular momentum and potential vorticity structure in GCM simulations. J. Atmos. Sci. 53, 3143–3156.

Beebe, R.F., Simon, A.A., Huber, L.F., 1996. Comparison of Galileo probe and Earth-based translation rates of Jupiter's equatorial clouds. Science 272, 841.

Bohren, C.F., Albrecht, B.A., 1998. Atmospheric Thermodynamics. Oxford University Press, New York.

Busse, F.H., 1983a. Convection-driven zonal flows in the major planets. Pure and Appl. Geophys. 121, 375–390.

Busse, F.H., 1983b. A model of mean zonal flows in the major planets. Geophys. Astrophys. Fluid Dyn. 23, 153–174.

Cess, R.D., Khetan, S., 1973. Radiative transfer within the atmospheres of the major planets. J. Quant. Spectrosc. Rad. Transfer 13, 995–1009.

Charney, J.G., Stern, M.E., 1962. On the instability of internal baroclinic jets in a rotating atmosphere. J. Atmos. Sci. 19, 159–172.

Cho, J.Y.K., Polvani, L.M., 1996. The morphogenesis of bands and zonal winds in the atmospheres on the giant outer planets. Science 273, 335–337.

Clarke, A.C., 1973. A meeting with Medusa. In: Pohl, C., Pohl, F. (Eds.), Jupiter. Ballantine Books, New York.

Condie, S.A., Rhines, P.B., 1994. A convective model for the zonal jets in the atmospheres of Jupiter and Saturn. Nature 367, 711–713.

Conrath, B.J., Flasar, F.M., Pirraglia, J.A., Gierasch, P.J., Hunt, G.E., 1981. Thermal structure and dynamics of the Jovian atmosphere. 2. Visible cloud features. J. Geophys. Res. 86, 8769–8775.

Del Genio, A.D., McGrattan, K.B., 1990. Moist convection and the vertical structure and water abundance of Jupiter's atmosphere. Icarus 84, 29–53.

Droegemeier, K., Sasamori, T., 1983. A linear analysis on the acceleration of zonal flow by baroclinic instability. Part II: Jovian atmosphere. J. Atmos. Sci. 40, 2339–2348.

Eliassen, A., Kleinschmidt, E., 1957. Dynamic meteorology. In: Flügge, S. (Ed.), Handbuch der Physik 48, Geophysik II. Springer-Verlag, Berlin, pp. 1–154.

Ertel, H., 1942. Ein Neuer hydrodynamischer Wirbelsatz. Meteor. Z. 59, 271–281.

Gierasch, P.J., 1976. Jovian meteorology: large-scale moist convection. Icarus 29, 445–454.

Gierasch, P.J., Conrath, P.J., 1985. Energy conversion processes in the outer planets. In: Hunt, G. (Ed.), Recent Advances in Planetary Meteorology. Cambridge University Press, Cambridge, pp. 121–146.

Gierasch, P.J., Conrath, B.J., Magalhaes, J.A., 1986. Zonal mean properties of Jupiter's upper troposphere from Voyager infrared observations. Icarus 67, 456–483.

Gierasch, P.J., Conrath, B.J., 1993. Dynamics of the atmospheres of the outer planets: post-Voyager measurement objectives. J. Geophys. Res. 98, 5459–5469.

Guillot, T., Gautier, D., Chabrier, G., Mosser, B., 1994. Are the giant planets fully convective? Icarus 112, 337–353.

Haltiner, G.J., Williams, R.T., 1980. Numerical Prediction and Dynamic Meteorology, 2nd ed. Wiley, New York.

Hammel, H.B., Beebe, R.F., Ingersoll, A.P., Orton, G.S., Mills, J.R., Simon, A.A., et al., 1995. HST imaging of atmospheric phenomena created by the impact of Comet Shoemaker–Levy 9. Science 267, 1288–1296.

Held, I.M., Hou, A.Y., 1980. Nonlinear axially symmetric circulations in a nearly inviscid atmosphere. J. Atmos. Sci. 37, 515–533.

Held, I.M., 1982. On the height of the tropopause and the static stability of the troposphere. J. Atmos. Sci. 39, 412–417.

Hide, R., 1966. On the circulation of the atmospheres of Jupiter and Saturn. Planet. Space Sci. 14, 669–675.

Hide, R., 1969. Dynamics of the atmospheres of the major planets with an appendix on the viscous boundary layer at the rigid bounding surface of an electrically-conducting fluid in the presence of a magnetic field. J. Atmos. Sci. 26, 841–853.

Hitchman, M.H., Leovy, C.B., 1986. Evolution of the zonal mean state in the equatorial middle atmosphere during October 1978–May 1979. J. Atmos. Sci. 43, 3159–3176.

Hoskins, B., 1991. Towards a PV-θ view of the general circulation. Tellus 43A (B), 27–35.

Hoskins, B.J., Pearce, R., 1983. Large-Scale Dynamical Processes in the Atmosphere. Academic Press, New York.

Hoskins, B.J., McIntyre, M.E., Robertson, A.W., 1985. On the use and significance of isentropic potential vorticity maps. Q. J. Roy. Met. Soc. 111, 877–946.

Huang, R.X., Stommel, H., 1990. Cross sections of a two-layer inertial Gulf Stream. J. Phys. Oceanogr. 20, 907–911.

Hunt, G.E., Conrath, B.J., Pirraglia, J.A., 1981. Visible and infrared observations of Jovian plumes during the Voyager encounter. J. Geophys. Res. 86, 8777–8781.

Ingersoll, A.P., Cuzzi, J.N., 1969. Dynamics of Jupiter's cloud bands. J. Atmos. Sci. 26, 981–985.

Ingersoll, A.P., Pollard, D., 1982. Motion in the interiors and atmospheres of Jupiter and Saturn: scale analysis, anelastic equations, barotropic stability criterion. Icarus 52, 62–80.

Ingersoll, A.P., Beebe, R.F., Conrath, B.J., Hunt, G.E., 1984. Structure and dynamics of Saturn's atmosphere. In: Gehrels, T., Matthews, M.S. (Eds.), Saturn. University of Arizona Press, Tucson, pp. 195–238.

Ingersoll, A.P., Miller, R.L., 1986. Motions in the interiors and atmospheres of Jupiter and Saturn. 2. Barotropic instabilities and normal modes of an adiabatic planet. Icarus 65, 370–382.

Ingersoll, A.P., Kanamori, H., Dowling, T.E., 1994. Atmospheric gravity waves from the impact of comet Shoemaker–Levy 9 with Jupiter. Geophys. Res. Lett. 21, 1083–1086.

Ingersoll, A.P., Kanamori, H., 1995. Waves from the collisions of comet Shoemaker–Levy 9 with Jupiter. Nature 374, 706–708.

Knox, J.A., Croft, P.J., 1997. Storytelling in the meteorology classroom. Bull. Am. Met. Soc. 78, 897–906.

Leovy, C., 1985. Eddy processes in the general circulation of the jovian atmospheres. In: Allison, M., Travis, L.D. (Eds.), The Jovian Atmospheres — NASA CP 2441. National Technical Information Service, Springfield, VA, pp. 177–192.

Limaye, S.S., 1986. Jupiter: new estimates of the mean zonal flow at the cloud level. Icarus 65, 335–352.

Lindal, G.F., Wood, G.E., Levy, G.S., Anderson, J.D., Sweetnam, D.N., Hotz, H.B., Buckles, B.J., Holmes, D.P., Doms, P.E., Eshleman, V.R., Tyler, G.L., Croft, T.A., 1981. The atmosphere of Jupiter: an analysis of the Voyager radio occultation measurements. J. Geophys. Res. 86, 8721–8727.

Maxworthy, T., 1985. Measurements and interpretation of a jovian, near-equatorial feature. Planet. Space Sci. 33, 987–991.

Niemann, H.B., Atreya, S.K., Carignan, G.R., Donahue, T.M., Haberman, J.A., Harpold, D.N., Hartle, R.E., Hunten, D.M., Kasprzak, W.T., Mahaffy, P.R., Owen, T.C., Way, S.H., 1998. The composition of the Jovian atmosphere as determined by the

Galileo probe mass spectrometer. J. Geophys. Res. 103, 22,831–22,845.

Oort, A.H., Rasmusson, E.M., 1971. Atmospheric Circulation Statistics. NOAA Professional Paper 5. US Department of Commerce, Rockville, MD.

Ortiz, J.L., Orton, G.S., Friedson, A.J., Stewart, S.T., Fisher, B.M., Spencer, J.R., 1998. Evolution and persistence of 5-μm hot spots at the Galileo probe entry latitude. J. Geophys. Res. 103, 23,051–23,069.

Orton, G.S., Fisher, B.M., Baines, K.H., Stewart, S.T., Friedson, A.J., Ortiz, J.L., Marinova, M., Ressler, M., Dayal, A., Hoffmann, W., Hora, J., Hinkley, S., Krishnan, V., Masanovic, M., Tesic, J., Tziolas, A., Parija, K.C., 1998. Characteristics of the Galileo probe entry site from Earth-based remote sensing observations. J. Geophys. Res. 103, 22,791–22,814.

Pedlosky, J., 1987. Geophysical Fluid Dynamics, 2nd ed. Springer Verlag, New York.

Pedlosky, J., 1996. Ocean Circulation Theory. Springer Verlag, New York.

Polvani, L.M., Wisdom, J., De Jong, E., Ingersoll, A.P., 1990. Simple dynamical models of Neptune' Great Dark Spot. Science 249, 1393–1398.

Read, P.L., 1986a. Stable, baroclinic eddies on Jupiter and Saturn: a laboratory analog and some observational tests. Icarus 65, 304–334.

Read, P.L., 1986b. Super-rotation and diffusion of axial angular momentum: II. A review of quasi-axisymmetric models of planetary atmospheres. Q. J. Roy. Met. Soc. 112, 253–272.

Sanchez-Lavega, A., Lecacheux, J., Colas, F., Laques, P., 1993. Temporal behavior of cloud morphologies and motions in Saturn's atmosphere. J. Geophys. Res. 98, 18,857–18,872.

Seiff, A., Kirk, D.B., Knight, T.C.D., Young, R.E., Mihalov, J.D., Young, L.A., Milos, F.S., Schubert, G., Blanchard, R.C., Atkinson, D., 1998. Thermal structure of Jupiter's atmosphere near the edge of a 5-μm hot spot in the north equatorial belt. J. Geophys. Res. 103, 22,857–22,889.

Showman, A.P., Ingersoll, A.P., 1998. Interpretation of Galileo probe data and implications for Jupiter's dry downdrafts. Icarus 132, 205–220.

Sromovsky, L.A., Revercomb, H.E., Krauss, R.J., Suomi, V.E., 1983. Voyager 2 observations of Saturn's northern mid-latitude cloud features: morphology, motions and evolution. J. Geophys. Res. 88, 8650–8666.

Sromovsky, L.A., Collard, A.D., Fry, P.M., Orton, G.S., Lemmon, M.T., Tomasko, M.G., Freedman, R.S., 1998. Galileo probe measurements of thermal and solar radiation fluxes in the Jovian atmosphere. J. Geophys. Res. 103, 22,929–22,977.

Stevens, D.E., 1983. On symmetric stability and instability of zonal mean flows near the equator. J. Atmos. Sci. 40, 882–893.

Stommel, H., 1954. Why do our ideas about the ocean circulation have such a peculiarly dream-like quality? or examples of types of observations that are badly needed to test oceanographic theories. In: Hogg, N.G., Huang, R.X. (Eds.), Collected Works of Henry M. Stommel, vol. I. American Meteorological Society, Boston Reprinted 1995.

Stommel, H., 1955. Discussion at the Woods Hole Convocation, June 1954. J. Mar. Res. 14, 504–510.

Stone, P.H., 1967. An application of baroclinic instability theory to the dynamics of the Jovian atmosphere. J. Atmos. Sci. 24, 642–652.

Stone, P.H., 1971. The symmetric baroclinic stability of an equatorial current. Geophys. Fluid Dyn. 2, 147–164.

Sun, D.Z., Lindzen, R.S., 1994. A PV view of the zonal mean distribution of temperature and wind in the extratropical troposphere. J. Atmos. Sci. 51, 757–772.

Sun, Z.P., Schubert, G., Glatzmaier, G.A., 1993. Banded surface flow maintained by convection in a model of the rapidly rotating giant planets. Science 260, 661–664.

Verne, J., 1877. Off on a Comet (English translation by Ellen E. Frewer). Edited to HTML by Zvi Har'El (http://JV.Gilead.org.il/pg/comet/).

Williams, G.P., 1975. Some ocean–Jupiter connections. Mode News 78, 1–4.

Williams, G.P., 1978. Planetary circulations: 1. Barotropic representation of Jovian and terrestrial turbulence. J. Atmos. Sci. 35, 1399–1426.

Williams, G.P., 1997. Planetary vortices and Jupiter's vertical structure. J. Geophys. Res. 102, 9303–9308.

Williams, G.P., Yamagata, T., 1984. Geostrophic regimes, intermediate solitary vortices, and Jovian eddies. J. Atmos. Sci. 41, 453–478.

Williams, G.P., Wilson, R.J., 1988. The stability and genesis of Rossby vortices. J. Atmos. Sci. 45, 207–241.

Young, R.E., 1998. The Galileo probe mission to Jupiter: science overview. J. Geophys. Res. 103, 22,775–22,790.

Zhang, K., Schubert, G., 1996. Penetrative convection and zonal flow on Jupiter. Science 273, 941–943.